Article

SOURCE DATA | TRANSPARENT PROCESS | OPEN ACCESS

THE EMBO JOURNAL

Post-transcriptional polyadenylation site cleavage maintains 3′-end processing upon DNA damage

Rym Sfaxi[1,2,3,†], Biswendu Biswas[1,2,3,4,5,†], Galina Boldina[1,2,3], Mandy Cadix[1,2,3], Nicolas Servant[6], Huimin Chen[7], Daniel R Larson[7], Martin Dutertre[1,2,3], Caroline Robert[4,5] & Stéphan Vagner[1,2,3,*]

Abstract

The recognition of polyadenylation signals (PAS) in eukaryotic pre-mRNAs is usually coupled to transcription termination, occurring while pre-mRNA is chromatin-bound. However, for some pre-mRNAs, this 3′-end processing occurs post-transcriptionally, i.e., through a co-transcriptional cleavage (CoTC) event downstream of the PAS, leading to chromatin release and subsequent PAS cleavage in the nucleoplasm. While DNA-damaging agents trigger the shutdown of co-transcriptional chromatin-associated 3′-end processing, specific compensatory mechanisms exist to ensure efficient 3′-end processing for certain pre-mRNAs, including those that encode proteins involved in the DNA damage response, such as the tumor suppressor p53. We show that cleavage at the p53 polyadenylation site occurs in part post-transcriptionally following a co-transcriptional cleavage event. Cells with an engineered deletion of the p53 CoTC site exhibit impaired p53 3′-end processing, decreased mRNA and protein levels of p53 and its transcriptional target p21, and altered cell cycle progression upon UV-induced DNA damage. Using a transcriptome-wide analysis of PAS cleavage, we identify additional pre-mRNAs whose PAS cleavage is maintained in response to UV irradiation and occurring post-transcriptionally. These findings indicate that CoTC-type cleavage of pre-mRNAs, followed by PAS cleavage in the nucleoplasm, allows certain pre-mRNAs to escape 3′-end processing inhibition in response to UV-induced DNA damage.

Keywords CoTC; polyadenylation; RNA 3′-end processing; TP53; ultraviolet irradiation

Subject Categories Chromatin, Transcription & Genomics; RNA Biology

DOI 10.15252/embj.2022112358 | Received 12 August 2022 | Revised 23 January 2023 | Accepted 25 January 2023 | Published online 10 February 2023

The EMBO Journal (2023) 42: e112358

Introduction

During UV-induced DNA damage and other genotoxic stresses, several steps in eukaryotic gene expression are repressed. Although global, this repression is associated with an upregulation of the expression of genes encoding proteins that are essential for the adaptation and response to stress. For instance, despite the inhibition of pre-mRNA 3′-end processing observed in UV-treated cells (Kleiman, 1999; Kleiman & Manley, 2001; Kim *et al*, 2006; Nazeer *et al*, 2011), pre-mRNA 3′-end processing of the pre-mRNA encoding the p53 tumor suppressor (TP53) protein is specifically maintained (Decorsière *et al*, 2011; Newman *et al*, 2017). This maintenance requires several RNA binding proteins, i.e., the heterogeneous nuclear ribonucleoprotein (hnRNP) F/H family of proteins that bind to an RNA G-quadruplex forming sequence located downstream of the p53 polyadenylation site (Decorsière *et al*, 2011), as well as the DHX36 RNA/DNA helicase (Newman *et al*, 2017).

The main mechanism of pre-mRNA 3′-end processing is cleavage and polyadenylation (CPA), which involves endonucleolytic cleavage of newly synthesized transcripts and the addition of adenosine residues constituting the poly(A) tail to the generated 3′-end. CPA is crucial for mRNA stability, transport to the cytoplasm, and translation (Millevoi & Vagner, 2010; Shi & Manley, 2015). This nuclear process involves the recognition of *cis*-acting elements in the pre-mRNA by a complex machinery comprising more than 80 proteins (Shi *et al*, 2009). The pre-mRNA sequences serving as the polyadenylation signal (PAS) include a hexameric sequence (most often AAUAAA) located 10–30 nucleotides (nt) upstream of the cleavage site (generally a CA dinucleotide) and a downstream sequence element (DSE; U/GU-rich) located within 30 nt downstream of the cleavage site. Additional sequence elements located either upstream (upstream sequence element; USE) or downstream (auxiliary downstream sequence element; AuxDSE) of the cleavage site modulate the recognition of the PAS.

The cleavage reaction at the PAS (called thereafter PAS cleavage), which precedes the addition of the poly(A) tail, generally

1 Institut Curie, PSL Research University, CNRS UMR3348, INSERM U1278, Orsay, France
2 Université Paris Sud, Université Paris-Saclay, CNRS UMR3348, INSERM U1278, Orsay, France
3 Equipe Labellisée Ligue Contre le Cancer, Paris, France
4 INSERM U981, Gustave Roussy, Gustave Roussy, Villejuif, France
5 Université Paris Sud, Université Paris-Saclay, Kremlin-Bicêtre, France
6 INSERM U900, Institut Curie, PSL Research University, Mines ParisTech, Paris, France
7 Laboratory of Receptor Biology and Gene Expression, National Cancer Institute, NIH, Bethesda, MD, USA
*Corresponding author. Tel: +33 169 86 31 03; E-mail: stephan.vagner@curie.fr
†These authors contributed equally to this work as first authors

occurs in a co-transcriptional manner. PAS recognition is indeed tightly coupled to RNA polymerase II (Pol II) transcription termination (Proudfoot, 2016). Rpb1, the largest subunit of Pol II, contains a carboxy-terminal domain (CTD) that is comprised of heptad repeats (consensus Tyr^1-Ser^2-Pro^3-Thr^4-Ser^5-Pro^6-Ser^7) and plays a critical role in coupling pre-mRNA 3′-end processing and transcription termination, especially through its phosphorylated Ser^2 (phospho-Ser^2) residues (Ahn *et al*, 2004). Several components of the polyadenylation machinery, including PCF11, which is concentrated at the 3′-end of genes, preferentially bind the phospho-Ser^2 CTD (Barilla *et al*, 2001; Licatalosi *et al*, 2002; Meinhart & Cramer, 2004). In human cells, PCF11 depletion leads to a transcription termination defect through a decrease in the degradation of the downstream RNA, generated after the PAS cleavage (West *et al*, 2008). In the Pause-Type model of transcription termination, Pol II pauses at a GC-rich region located a few nucleotides downstream of the PAS, stimulating the PAS cleavage of the pre-mRNA in a co-transcriptional manner, i.e., when the pol II-bound pre-mRNA is on the chromatin (Gromak *et al*, 2006; Nojima *et al*, 2013; Cortazar *et al*, 2019).

Another model of transcription termination has been proposed (Dye & Proudfoot, 2001; West *et al*, 2008; Nojima *et al*, 2013). In this Co-Transcriptional Cleavage (CoTC)-type model, the pre-mRNA is released from chromatin to nucleoplasm through a cleavage event at a CoTC site located downstream of the PAS, and the PAS cleavage subsequently occurs in the nucleoplasm. This mechanism has been described in several human genes (Nojima *et al*, 2013). The CoTC-type termination model has also been observed in *Drosophilia* where a release of pre-mRNA from transcription sites to the nucleoplasm takes place prior to PAS cleavage (Sikes *et al*, 2002). The CoTC cleavage occurs a few kilobases downstream of the PAS, generally at an AT-rich sequence called CoTC element (White *et al*, 2013). Mutations in this element induce an inhibition of pre-mRNA 3′-end processing *in vitro* (Teixeira *et al*, 2004).

Here, we report that upon UV irradiation, PAS cleavage of the *p53* pre-mRNA is independent from the cleavage/termination factor PCF11 and CTD Ser^2 phosphorylation and relies on a downstream CoTC site, thereby allowing 3′-end processing of the *p53* pre-mRNA to escape repression by DNA damage. We also identified several other pre-mRNAs that exhibit a CoTC-type mechanism of 3′-end processing in response to UV-induced DNA damage and that escape repression by DNA damage, like the *p53* pre-mRNA.

Results

PCF11 is dispensable for *p53* pre-mRNA 3′-end processing in UV-treated cells

To understand the contribution of the pre-mRNA 3′-end processing machinery in the response to UV treatment, we analyzed the abundance of 13 proteins constituting the different sub-complexes involved in 3′-end processing by Western blot (Fig 1A). To ascertain that the band observed in each Western blot corresponds to the expected protein, we used published siRNAs targeting each of the corresponding mRNAs (Masamha *et al*, 2014). The experiments were performed in A549 lung tumor cells irradiated with UV (254 nm; 40 J/m^2) and harvested after 16 h of recovery, conditions that we previously used to demonstrate the maintenance of *p53* pre-mRNA 3′-end processing following UV treatment (Decorsière *et al*, 2011; Newman *et al*, 2017). Consistent with previously reported data (Kleiman & Manley, 2001), we observed no changes in the levels of both CstF64 and CPSF160 in response to UV. The abundance of the other components of the CPSF, CstF, and CFIm complexes was unchanged (Fig 1A). By contrast, we detected a significant decrease in the abundance of both PCF11 and CLP1 in UV-treated cells (Fig 1A). The UV-dependent reduction in PCF11 expression was confirmed in another set of experiments using 2 different siRNAs targeting PCF11 (Fig 1B) and was accompanied by a 5-fold decrease in *PCF11* mRNA level (Fig 1C). These observations suggest that PCF11 might be dispensable for *p53* pre-mRNA 3′-end processing following UV-induced DNA damage.

To confirm that PCF11 is not required for *p53* pre-mRNA 3′-end processing following UV, we evaluated the effect of the siRNA-mediated depletion of PCF11 on the efficiency of PAS cleavage of the *p53* pre-mRNA by real-time quantitative PCR analysis (RT–qPCR; Fig 1D). The *TBP* pre-mRNA was used as a control since it was previously shown to be inhibited at the level of PAS cleavage efficiency due to UV treatment (Decorsière *et al*, 2011; Newman *et al*, 2017). According to a previously described approach (Decorsière *et al*, 2011; Newman *et al*, 2017), we measured the ratio of uncleaved RNA to total RNA (that is the sum of cleaved and uncleaved RNA) in the nuclear pool of RNAs, by qPCR with antisense primers located either downstream or upstream of the PAS cleavage site, respectively (Fig 1D). In untreated cells, PAS cleavage of both the *TBP* and *p53* pre-mRNAs was inhibited by PCF11 depletion, as revealed by the increased ratio of uncleaved/total RNAs in PCF11-depleted cells (Fig 1E). This is consistent with the fact that this factor is essential for the co-transcriptional, Pol II-coupled PAS cleavage reaction (West *et al*, 2008). Following UV treatment, while *TBP* PAS cleavage was still inhibited by PCF11 depletion, *p53* PAS cleavage was no longer inhibited (Fig 1E). This effect was specific to PCF11 since the siRNA-mediated depletion of CstF64, CFIm25, and CPSF160 all led to decreased *p53* PAS cleavage in UV-treated cells (Appendix Fig S1). Altogether, these data indicate that PCF11, which exhibits reduced RNA and protein levels in UV-treated cells, is dispensable for *p53* (but not *TBP*) pre-mRNA 3′-end processing in UV-treated cells.

Previous reports showed that UV-induced DNA damage induces global changes in Pol II phosphorylation, including Ser^2 phosphorylation (Rockx *et al*, 2000; Muñoz *et al*, 2009). Considering the link between PCF11 and the Pol II CTD phospho-Ser^2 (PolII Ser2P), we sought to determine whether inhibition of Ser^2 phosphorylation may mimic the effect of depleting PCF11 on *p53* 3′-end processing following UV. We treated cells with the Ser^2 kinase (CDK9) inhibitor DRB (5,6-Dichlorobenzimidazole 1-β-D-ribofuranoside) and then assessed the efficiency of pre-mRNA 3′-end processing. DRB reduced Pol II Ser^2 phosphorylation (Fig EV1A). DRB, as expected, inhibited both *TBP* and *p53* PAS cleavage in untreated cells (Fig EV1B). In UV-treated cells, DRB inhibited *TBP*, but not *p53* PAS cleavage (Fig EV1C).

PAS cleavage of the *p53* pre-mRNA occurs in the nucleoplasm following a CoTC event

The experiments above show that, in UV-treated cells, PAS cleavage of the *p53* pre-mRNA does not require PCF11 and Pol II CTD

phospho-Ser[2]. This suggests that it might occur in a transcription termination uncoupled manner, as described in the CoTC-type model, where PAS cleavage occurs post-transcriptionally, following a co-transcriptional cleavage at a downstream CoTC site (Nojima *et al*, 2013). In this case, a pre-mRNA that has not undergone PAS cleavage (PAS-uncleaved pre-mRNA) can be detected in the

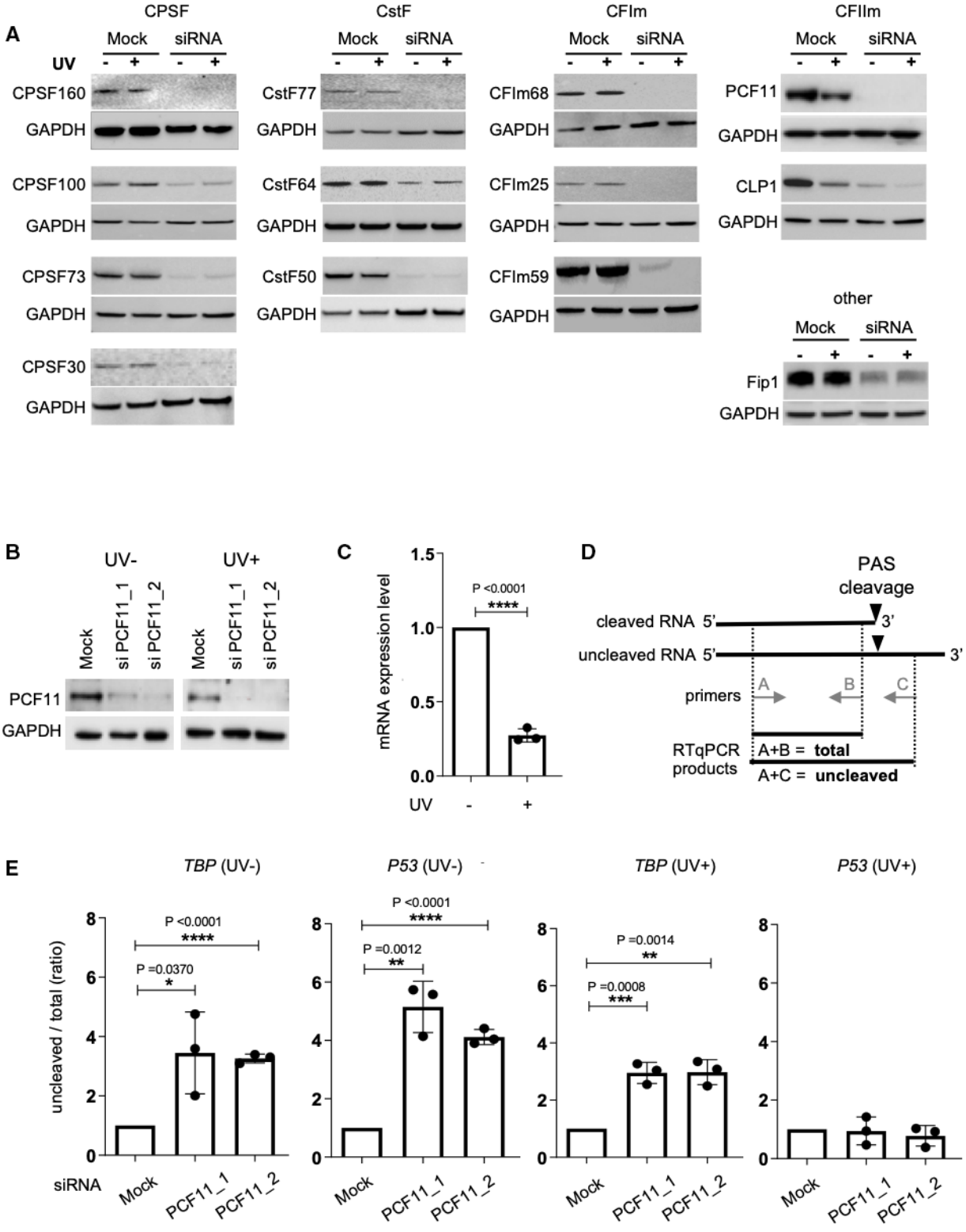

Figure 1.

Figure 1. PCF11 is dispensable for *p53* pre-mRNA 3′-end processing in UV-treated cells.

A Western blot of pre-mRNA 3′-end processing factors in response to UV treatment (40 J/m^2) of A549 cells (n = 3), followed by 16 h of recovery. GAPDH was used as a loading control.

B Western blot analysis of PCF11 expression in A549 cells (n = 3) transfected for 48 h with two different siRNA targeting PCF11 prior to exposure to UV.

C RT–qPCR measuring relative PCF11 mRNA level (n = 3) in A549 cells in response to UV treatment (40 J/m^2). The expression was normalized to RP18S.

D Scheme representing the RT–qPCR strategy for assessing pre-mRNA 3′-end processing efficiency. Primers for uncleaved pre-mRNAs are located downstream of the polyadenylation site, while primers that detect both processed (cleaved) and unprocessed RNAs (uncleaved) amplify upstream of the polyadenylation site. The ratio of uncleaved/total (cleaved + uncleaved) indicates the processing efficiency, where a greater uncleaved/total ratio represents a reduced processing.

E RT–qPCR assay on nuclear RNA for assessing the uncleaved/total ratio of *p53* and TATA-binding protein (*TBP*) pre-mRNAs in A549 cells (n = 3) transfected for 48 h with two different siRNA targeting PCF11 prior to exposure (UV+) or not (UV−) to UV irradiation (40 J/m^2).

Data information: "n" indicates the number of biological replicates for each experiment. All data are presented as the mean ± s.e.m. P-values were calculated using a two-sided unpaired t-test.
Source data are available online for this figure.

nucleoplasm, where it is released upon CoTC cleavage. We therefore analyzed the nuclear distribution of the PAS-uncleaved *p53* pre-mRNA by RT–qPCR in chromatin and nucleoplasm fractions. The quality of the fractionation was assessed by Western blot against histone H3 as a chromatin marker and topoisomerase IIα as a nucleoplasm marker (Fig 2A). The *GAPDH* and *WDR13* pre-mRNAs were used as controls as they were previously reported to be PAS-cleaved co-transcriptionally or post-transcriptionally (following a CoTC event), respectively (Nojima *et al*, 2013). Accordingly, the relative abundance of PAS-uncleaved pre-mRNA in the nucleoplasm, as compared to the chromatin, was much higher for *WDR13* than for *GAPDH* (Fig 2B). The nucleoplasm/chromatin ratio of PAS-uncleaved pre-mRNA of *p53* was similar to the one of *WDR13*, suggesting that the *p53* pre-mRNA may be released in the nucleoplasm following a CoTC event, while the *TBP* pre-mRNA behaved similarly to the *GAPDH* pre-mRNA (Fig 2B).

An AT-rich sequence that could correspond to a potential CoTC sequence element is found around 1,200 nt downstream of the *p53* PAS (Fig 2C). To map the putative CoTC element, chromatin-associated RNA was reverse transcribed using random primers and the obtained cDNA was amplified by PCR using primers complementary to the 3′ flanking region of the *p53* gene (Fig 2C). PCR amplification was carried out using a single forward primer (F), located upstream of the *p53* PAS, in combination with reverse primers (R1-R6) located at an increasing distance downstream of the *p53* PAS. The F/(R1-R6) primer pairs were used to amplify genomic DNA as an amplification control (Fig 2D). In cDNA derived from chromatin-bound RNA, the F-R1, F-R2, F-R3, and F-R4 primer pairs resulted in the detection of PCR products at the expected size of 229, 558, 852, and 1,000 bp (Fig 2D; lanes 7–10). Of note, these PCR products precisely correspond to bands obtained with genomic DNA (lanes 1–4). By contrast, the F-R5 and F-R6 primer pairs did not yield detectable PCR products with cDNA samples from chromatin-bound RNA (lanes 11–12) even though PCR products were obtained with the genomic DNA control (lanes 5–6). These observations indicate that the *p53* pre-mRNA is cleaved in between approximately 1,000 to 1,400 nt downstream of the PAS, in the region where the AT-rich sequence is located. To ascertain that this cleavage event is not linked to the presence of an alternative PAS, we adopted the same mapping strategy using chromatin-bound pre-mRNA, but reverse transcription was performed with an oligo-dT primer. A cDNA derived from an mRNA transcript was included as a control. No bands were detected with all primer pairs used previously, except for the control (Fig 2E). In addition, nucleoplasmic RNA was reverse transcribed using random primers and the obtained cDNA was amplified by PCR as in Fig 2C. The bands obtained show that the CoTC-cleaved RNA can be detected in the nucleoplasm (Fig 2F). Altogether, these data indicate that the *p53* pre-mRNAs cleaved in the vicinity of the AT-rich region (i) do not contain a poly(A) tail, (ii) are generated through a CoTC-type event in a UV-induced manner, and (iii) can be found in the nucleoplasm before PAS cleavage.

Consistently, using single-molecule fluorescence in these *in situ* hybridization (smFISH; Fig 3A), we found that *p53* pre-mRNA regions downstream of the PAS (probe B) were detected following UV exposure (median number of smFISH spots: no UV = 7; with UV = 6, with n = 1,797 and 2,165 cells, respectively; Fig 3B and Appendix Fig S2). This is not true for *GAPDH* (probe D), as expected for a pre-mRNA that undergoes efficient co-transcriptional PAS cleavage and no CoTC-type cleavage. Without UV exposure, *GAPDH* downstream regions targeted by probe D were visible and localized to the transcription sites (46% cells containing 1 or more active sites, n = 8,448 cells; Fig 3B). However, following UV exposure, the downstream regions targeted by probe D were observed less frequently in the nucleus (26% cells containing 1 or more active sites, n = 6,481 cells). It is possible that these GAPDH spots in the nucleus reflect transcription past the termination sequence, which is now understood to be widespread (Vilborg *et al*, 2015). Notably, we rarely observed more than 3 such sites (< 5% of cells), which is consistent with chromatin-bound transcripts at the site of synthesis in stark contrast to the more abundant p53 nuclear transcripts. Finally, RNA regions upstream of the PAS were detected for both *p53* (probe A; median number of smFISH spots: no UV = 18; with UV = 26, with n = 1,797 and 2,165 cells, respectively) and *GAPDH* (probe C; Fig 3B), as expected for mature mRNAs. Thus, our smFISH data are consistent with our RT–qPCR data on chromatin (Fig 2) indicating that PAS cleavage of *p53* pre-mRNA occurs post-transcriptionally.

Of note, we have previously shown that hnRNP H/F (Decorsière *et al*, 2011) and DHX36 (Newman *et al*, 2017) are involved in the regulation of *p53* pre-mRNA 3′-end processing following UV-induced DNA damage. Consistent with *p53* pre-mRNA 3′-end processing mostly occurring in the nucleoplasm, the increased uncleaved/total ratio of *p53* pre-mRNA following the depletion of DHX36 or hnRNP H/F was significantly higher in the nucleoplasm than in the chromatin (Appendix Fig S3).

The CoTC site is implicated in the maintenance of *p53* pre-mRNA 3′-end processing in response to UV-induced DNA damage

In order to determine the importance of the CoTC site in *p53* pre-mRNA 3′-end processing following UV, the *p53* CoTC element was deleted using a CRISPR-based strategy in both A549 lung tumor and A375 melanoma cells (Appendix Fig S4A). We obtained an A549 clone with deletion of the CoTC site in all three *TP53* alleles existing in these cells (hereafter called ΔCoTC) and several A549 and A375 clones with deletion of only a subset of alleles (hereafter called pΔCoTC; Appendix Fig S4B). ΔCoTC, pΔCoTC, and WT cells were then tested for *p53* pre-mRNA 3′-end processing efficiency in response to UV.

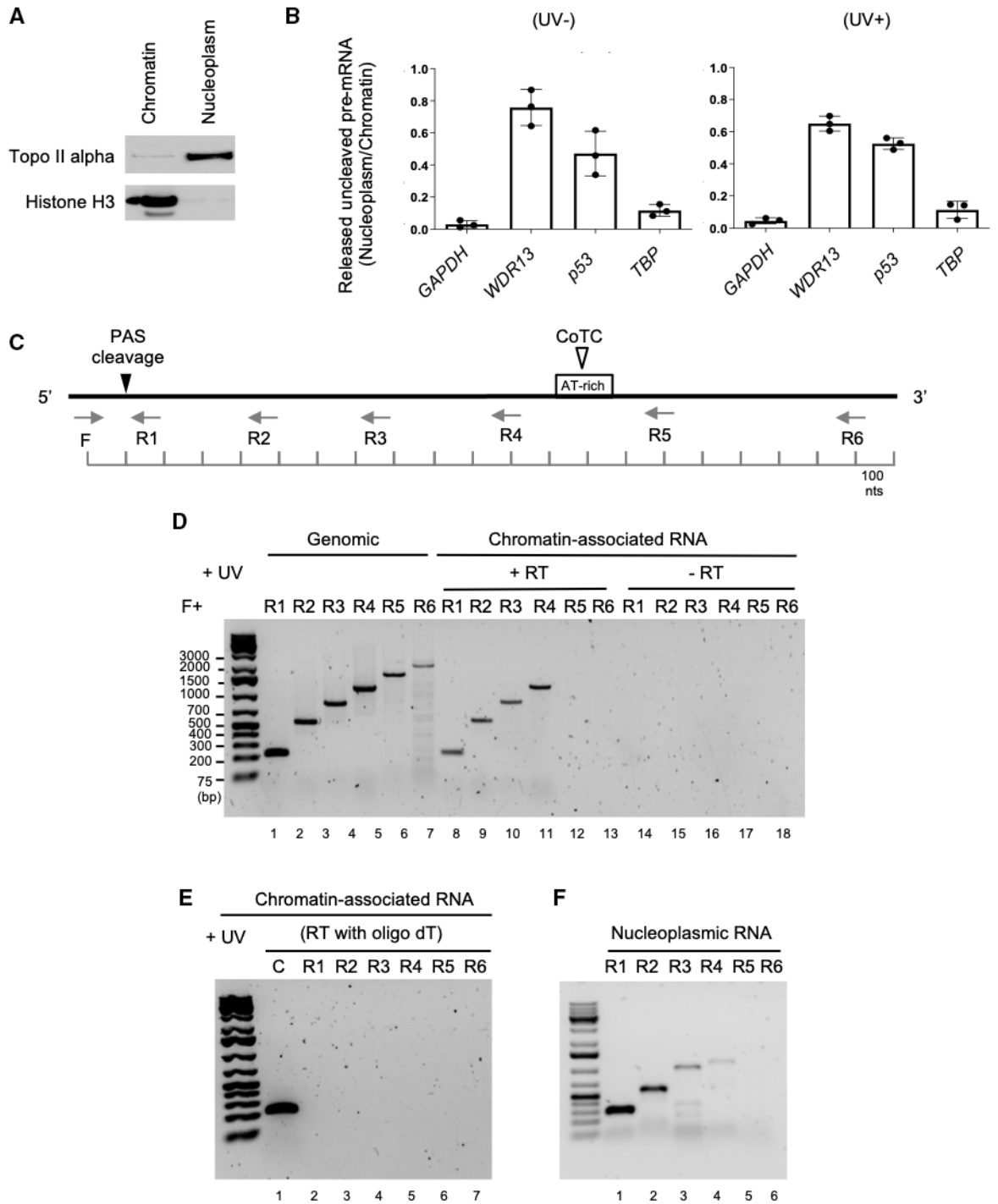

Figure 2.

Figure 2. p53 pre-mRNA 3′-end cleavage occurs in the nucleoplasm following a CoTC.

A Western blot analysis to verify the quality of the nuclear fractionation of UV-treated A549 cells ($n = 3$; 40 J/m^2). The topoisomerase II alpha was used as a marker of the nucleoplasm compartment and the histone H3 for the chromatin fraction.

B RT–qPCR analysis on RNA extracted from nucleoplasm and chromatin fractions. The ratio of uncleaved pre-mRNA (nucleoplasm/chromatin) was calculated to quantify the level of unprocessed *p53*, *TBP*, *WDR13* and *GAPDH* pre-mRNA ($n = 3$ biological replicates) released in the nucleoplasm compared with the chromatin-bound unprocessed pre-mRNA. *WDR13* and *GAPDH* were included as controls as they have been previously reported to be processed post- and co-transcriptionally, respectively. Data are presented as the mean ± s.e.m.

C Scheme representing the strategy to map the location of the CoTC site in the *p53* pre-mRNA. Forward primer (F) is located upstream of the PAS (poly(A) site) and reverse primers (R1-6) are located downstream at increasing distances from the PAS.

D RT–PCR analysis of p53 3′ flanking region using primer pairs indicated (black arrows) in the scheme above the data panel ($n = 3$). Lanes 1–6 correspond to amplified genomic DNA used as a PCR amplification control. Lanes 7–12 correspond to cDNA derived from chromatin-associated RNA reverse transcribed (+RT) using random primer. Lanes 13–18 are negative RT control samples (−RT).

E RT–PCR analysis of *p53* 3′ flanking region using the same primers employed in the data panel above ($n = 3$). Lane 1 is a control PCR amplification of cDNA derived from the reverse transcription of a control mRNA using oligo (dT). Lanes 2–7 are PCR amplification of reverse transcribed p53 chromatin-associated pre-mRNA using oligo oligo (dT).

F RT–PCR analysis of p53 3′ flanking region ($n = 3$). cDNAs were derived from nucleoplasmic-associated RNA reverse transcribed using random primer.

Source data are available online for this figure.

We observed an increase in the PAS-uncleaved to total ratio for *p53* in UV-treated ΔCoTC but not WT cells (Fig 4A). Similar results were obtained with pΔCoTC A549 (Appendix Fig S5A) and pΔCoTC A375 (Appendix Fig S5B) cells. As a control, the deletion of the *p53* CoTC region had no effect on the UV-dependent regulation of pre-mRNA 3′-end processing for *WDR13*, *GAPDH*, and *TBP* (Fig 4A and Appendix Fig S5). Thus, the *p53* CoTC region is required for the maintenance of *p53* pre-mRNA 3′-end processing upon UV exposure. We also found a decrease in the nucleoplasm/chromatin ratio of the *p53* PAS-uncleaved pre-mRNA in ΔCoTC cells when compared to WT cells (Fig 4B). This effect was also observed in pΔCoTC A549 (Appendix Fig S6A) and pΔCoTC A375 (Appendix Fig S6B) cells and was not observed for the *WDR13*, *GAPDH*, and *TBP* pre-mRNAs (Fig 4B and Appendix Fig S6). This shows that the *p53* CoTC site is required for the release of the PAS-uncleaved *p53* pre-mRNA from chromatin to nucleoplasm in response to UV. Consistently, total *p53* mRNA levels were decreased in ΔCoTC and pΔCoTC cells, but not in WT cells, in response to UV (Fig 4C and Appendix Fig S7A). In addition, the UV-dependent increase in p53 protein levels in WT cells was not observed in ΔCoTC and pΔCoTC cells (Fig 4D and Appendix Fig S7B). Altogether, these data show that the CoTC site of *p53* is required to maintain *p53* PAS cleavage and promote *p53* expression following UV irradiation.

We then assessed the potential consequences of CoTC site deletion on downstream functions of p53. A direct transcriptional target of the p53 protein is the *CDKN1A/p21* gene, which encodes an inhibitor of cell cycle progression from G1 to S phase (Jeong *et al*, 2010; Galanos *et al*, 2016; Matsuda *et al*, 2017). UV-induced upregulation of *p21* mRNA and p21 protein levels was observed in WT cells but not in ΔCoTC and pΔCoTC cells (Fig 4C and D, and Appendix Fig S7A and B). Analysis of cell cycle distribution by FACS showed no effect of CoTC site deletion in the absence of UV (Fig 4E, left panels). However, a moderate UV treatment, which had no effect on cell cycle distribution in WT cells, led to a decrease in G0/G1 cells in ΔCoTC and pΔCoTC cells (Fig 4E and Appendix Fig S8). Altogether, these data suggest that deletion of the *p53* CoTC site leads to impaired p21 induction and enhanced G1-S phase progression following moderate UV irradiation.

The 3′-end processing of several pre-mRNAs undergoing a CoTC cleavage event is maintained in response to UV-induced DNA damage

Our finding that the CoTC site of *p53* pre-mRNA is required for *p53* to escape 3′-end processing inhibition by UV prompted us to investigate whether CoTC-dependent cleavage may be linked to UV-resistant pre-mRNA 3′-end processing in other genes. Toward this aim, we first developed a strategy to analyze in a high-throughput manner the efficiency of pre-mRNA 3′-end cleavage by RNA-sequencing (RNA-Seq). This strategy is based on the evaluation of the number of reads located in 500 nt-long windows either upstream (total RNA) or downstream of the PAS (PAS-uncleaved RNA; Fig 5A). An increase in the ratio of downstream reads to upstream reads indicates inhibition of 3′-end cleavage, leading to read-through transcription (Vilborg *et al*, 2015). Focusing on 4,208 expressed genes (Dataset EV1) with detectable reads downstream of the PAS and using a cut-off of $P < 0.05$, this analysis identified 378 pre-mRNAs with UV-repressed 3′-end processing and 108 pre-mRNAs with a more efficient 3′-end processing in UV-treated compared with untreated cells (UV-resistant 3′-end processing; Fig 5B). Examples of the read distribution in the 500 nt-long windows located upstream and downstream of the PAS are illustrated in Fig 5C for the *ZRANB2* and the *HMGB1* genes. In the case of *ZRANB2* that belongs to the UV-repressed 3′-end processing group, the absence of reads downstream of the PAS in untreated cells indicates a very efficient 3′-end processing activity, while the presence of more reads in this window in UV-treated cells indicates a reduced 3′-end processing efficiency following UV treatment. In the case of *HMGB1* that belongs to the UV-resistant 3′-end processing group, we observed an opposite trend showing that there is an increase in pre-mRNA 3′-end processing following UV treatment (Fig 5C).

We randomly chose 9 candidate genes from each group and validated the RNA-Seq data by RT–qPCR on PAS-uncleaved and total RNA using primers located downstream or upstream of the PAS, respectively (Fig 6A). These RT–qPCR analyses showed that all candidate pre-mRNAs of the UV-repressed group exhibited 3′-end processing inhibition by UV (Fig 6A, red bars). By contrast, all

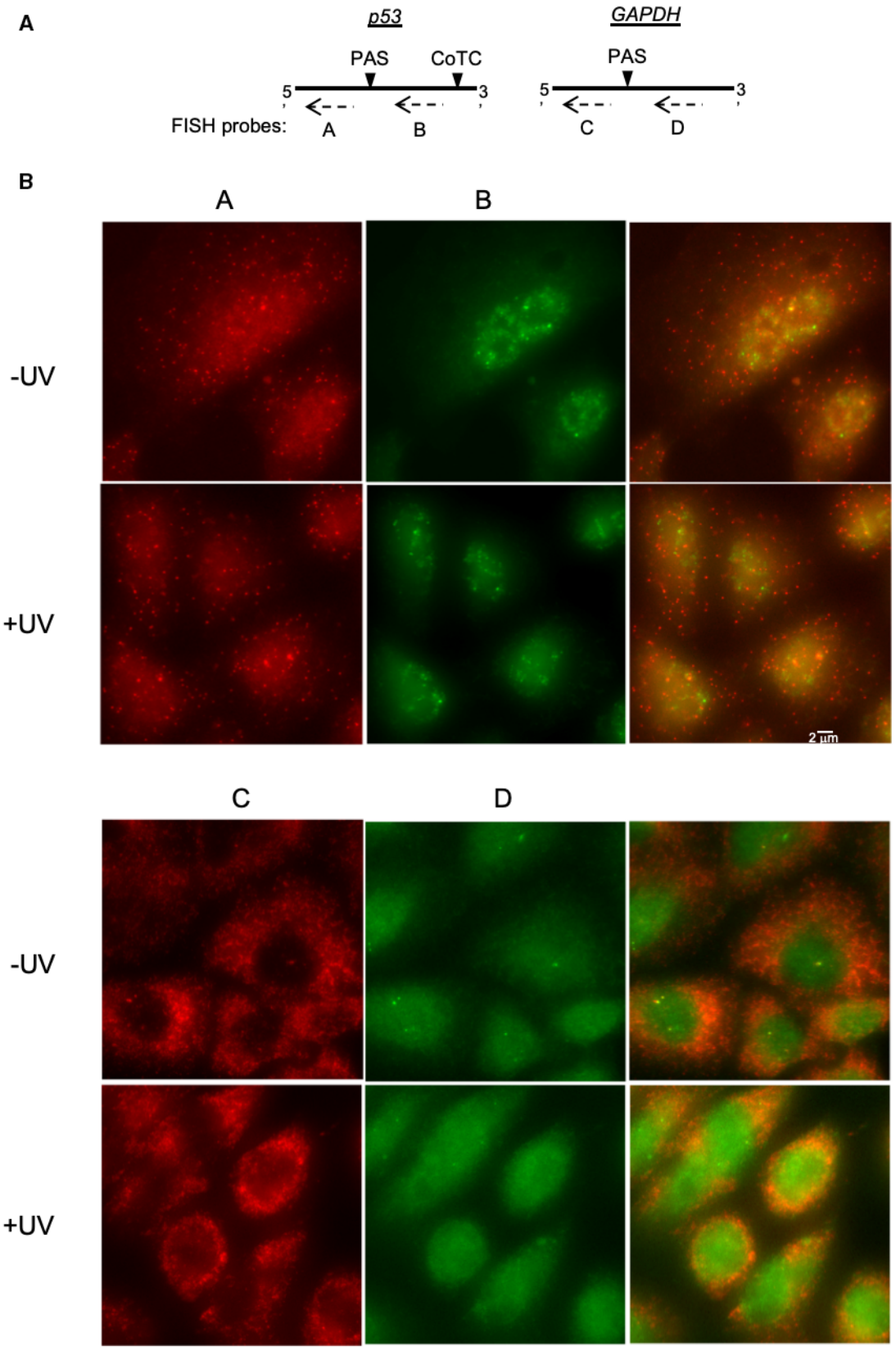
A
p53
PAS
CoTC
5
3
FISH probes:
A
B
GAPDH
PAS
5
3
C
D
B
A
B
-UV
+UV
2 µm
C
D
-UV
+UV

Figure 3.

Figure 3. PAS cleavage of *p53* pre-mRNA occurs post-transcriptionally.

A Probe design for single-molecule Fluorescence *in situ* hybridization (smFISH) spanning regions upstream "A" and downstream "B" of *p53* PAS, as well as those spanning regions upstream "C" and downstream "D" of *GAPDH* PAS.

B Representative images of smFISH in untreated (−UV) or UV-treated (+UV) A549 cells with the indicated probes (A, B, C, and D).

candidate pre-mRNAs of the UV-resistant group were resistant to 3′-end processing inhibition by UV (Fig 6A, blue bars). These include several DDR-related genes, namely XRCC5 and HMGB1. Because our RNA-seq approach is limited by the sensitivity of read detection downstream of the PAS, we also analyzed six genes from the p53 pathway by RT–qPCR. One of them (i.e., *NOXA*) exhibited 3′-end processing inhibition by UV, while four genes escaped repression (i.e., *MDM2*, *PUMA*, *PTEN*, and *FAS*; Fig 6A, right). Altogether, our RT–qPCR analyses identified 15 pre-mRNAs that were resistant to 3′-end processing inhibition by UV, and 12 pre-mRNAs that underwent inhibition.

Then, we measured by RT–qPCR the nucleoplasm/chromatin ratio of PAS-uncleaved pre-mRNA. Remarkably, all 15 UV-resistant pre-mRNAs had a high nucleoplasm/chromatin ratio, indicating that PAS cleavage occurs at least in part post-transcriptionally (Fig 6B). By contrast, none of the 12 UV-repressed pre-mRNAs were abundant in the nucleoplasm (Fig 6B). These data show that resistance of PAS cleavage to UV correlates with its occurrence in the nucleoplasm, thus extending our findings on *p53*.

Because we found that the UV resistance and nucleoplasmic occurrence of the *p53* pre-mRNA PAS cleavage require a downstream CoTC cleavage site (Fig 3), we then used our PCR-based mapping strategy (Fig 2) to locate putative CoTC elements in eight other UV-resistant pre-mRNAs (Appendix Fig S9A and B). For the eight tested genes, the presence of CoTC cleavage sites was validated by the sharp loss of amplification at a given distance (most often about 2.5 kb) downstream of the PAS (Appendix Fig S9C). As for *p53* (Fig 2E), the CoTC-dependent cleavage event for the eight tested genes is not linked to the presence of an alternative PAS (Appendix Fig S9D).

Gene Ontology (GO) analysis of pre-mRNAs with a more efficient 3′-end processing in UV-treated compared with untreated cells shows an enrichment of genes involved in the inhibition of apoptosis and processes related to two genotoxic stress-inducing agents, doxorubicin and daunorubicin (Fig EV2). Since we previously showed that *p53* pre-mRNA 3′-end processing is maintained upon doxorubicin treatment (Decorsière *et al*, 2011), we studied the involvement of a CoTC-based regulation in doxorubicin-treated cells. We observed an increase in the PAS-uncleaved to total ratio for *p53* in UV-treated ΔCoTC and pΔCoTC but not in A549 WT cells (Fig EV3 and Appendix Fig S10). Thus, the *p53* CoTC region is required for the maintenance of *p53* pre-mRNA 3′-end processing upon doxorubicin treatment. In addition, RT–qPCR analyses showed that 11 out of 12 UV-repressed pre-mRNAs also exhibited 3′-end processing inhibition by doxorubicin and that all 15 pre-mRNAs of the UV-resistant group were also resistant to 3′-end processing inhibition by doxorubicin (Appendix Fig S11). Altogether, these results provide evidence for an association between maintained 3′-end processing following UV irradiation/doxorubicin treatment and the presence of a CoTC element in several genes including DDR-related genes (*XRCC5*, *PUMA*, *FAS*, *MDM2*, *TP53*).

Discussion

Pre-mRNA 3′-end processing by PAS cleavage and poly(A) tail addition mostly occurs in a co-transcriptional manner. We show here that PAS cleavage of the *p53* pre-mRNA occurs at least in part in a manner that is uncoupled from transcriptional termination. It involves a CoTC sequence that lies about 1.2 kb downstream of the PAS and allows a first 3′-end cleavage event, leading to the dissociation of the pre-mRNA from chromatin. This is followed by a second 3′-end cleavage event (and polyadenylation) occurring at the PAS of the released RNA in the nucleoplasm.

One of the important factors in the coupling between 3′-end processing and transcription termination is PCF11, a 3′-end processing factor that mediates transcriptional termination in yeast (Grzechnik *et al*, 2015; Larochelle *et al*, 2018), as well as in vertebrates (Kamieniarz-Gdula *et al*, 2019). PCF11 recruits the yeast Rat1 or human Xrn2 exonucleases to exert a 5′-3′ exonucleolytic degradation on the nascent RNA leading Pol II to terminate transcription (Luo, 2006; West & Proudfoot, 2007; Eaton *et al*, 2018). We show that pre-mRNA 3′-end processing is inhibited in the absence of PCF11 (Fig 1). PCF11 interacts with CLP1 to target the cleavage site and modulates the binding and cleavage efficiency of CFII (Zhang *et al*, 2021). It also regulates polyadenylation site choice and plays a role in controlling the 3′ Untranslated Region (3′UTR) of transcripts (Ogorodnikov *et al*, 2018; Wang *et al*, 2019; Nourse *et al*, 2020). However, *p53* pre-mRNA 3′-end processing is independent of PCF11 in UV-treated cells, allowing this pre-mRNA to escape from the decrease in PCF11 levels observed in UV-treated cells (Fig 1). Since PCF11 has a CTD Interacting Domain (CID) and binds preferentially the phosphorylated Ser2 of an elongating RNAP II (Meinhart & Cramer, 2004), our results clearly indicate an uncoupling of 3′-end processing and transcriptional termination in the p53 pre-mRNA following UV-induced DNA damage.

We demonstrate that *p53* pre-mRNA 3′-end processing does not require PCF11 because it is processed at a CoTC sequence (Figs 2 and 3). CRISPR-based deletion of the p53 CoTC leads to inhibition of *p53* pre-mRNA 3′-end processing, decreased p53 and p21 protein levels, and decreased G0/G1 cells in UV-treated cells (Fig 4). This is consistent with the fact that UV radiation-induced cell cycle arrest is correlated with increase in p53 levels (Latonen *et al*, 2001) and causes retention of cells at the G2-M phase (Céraline *et al*, 1998; van Oosten *et al*, 2000; Pavey *et al*, 2001; Blackford & Jackson, 2017). CoTC-dependent cleavage therefore acts as a mechanism of escape from UV-induced global inhibition of pre-mRNA 3′-end processing. Beyond *p53*, the presence of CoTC elements in the 3′ flanking regions of a number of genes, including genes implicated in p53-mediated DNA damage response, was validated (Figs 5 and 6).

We thus propose a model where UV-induced or doxorubicin-triggered DNA damage inhibits co-transcriptional PAS cleavage, which is chromatin-bound and PCF11-dependent, but not post-

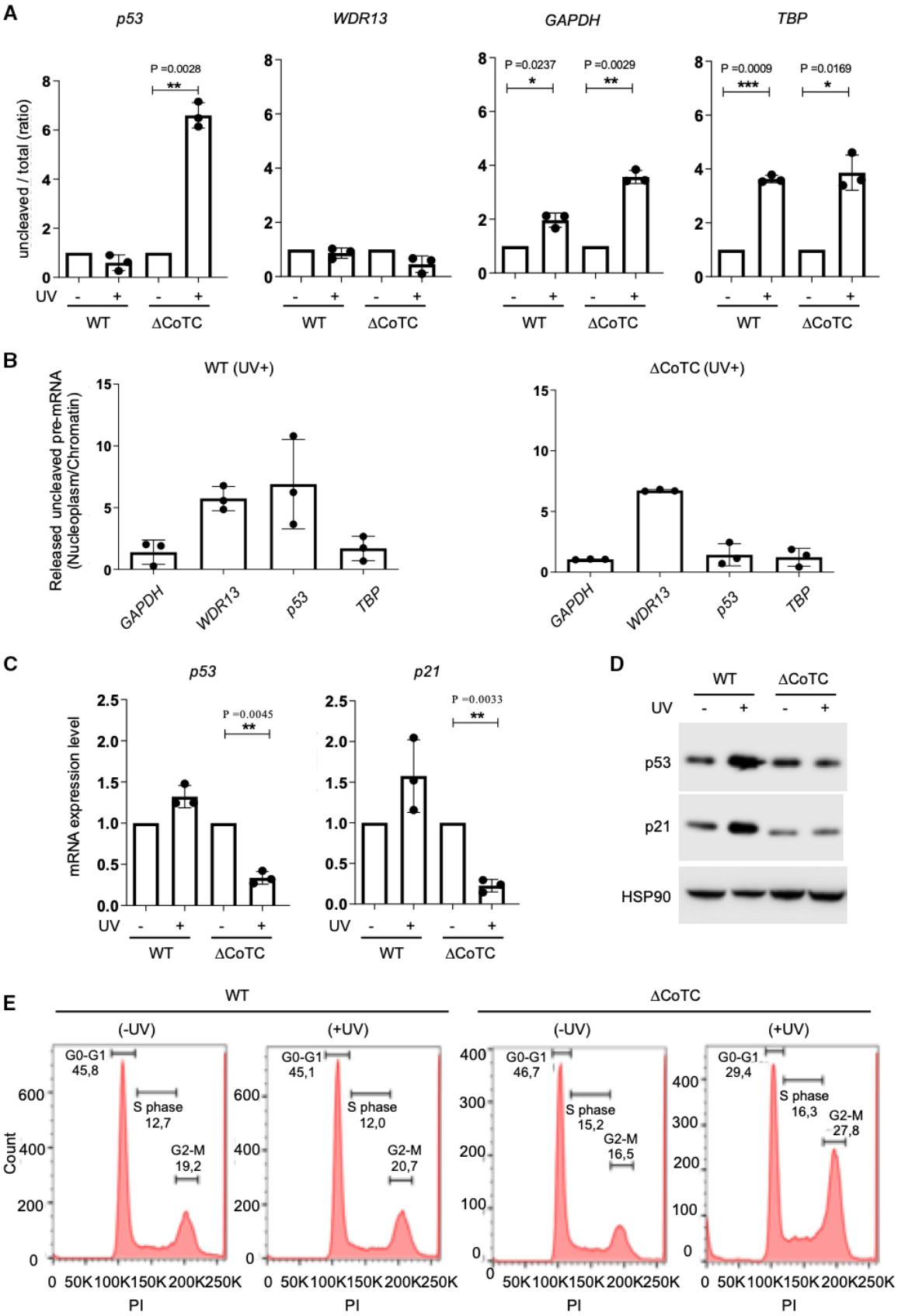
A
p53
WDR13
GAPDH
TBP
uncleaved / total (ratio)
P =0.0028
P =0.0237
P =0.0029
P =0.0009
P =0.0169
UV
WT
ΔCoTC
B
WT (UV+)
ΔCoTC (UV+)
Released uncleaved pre-mRNA (Nucleoplasm/Chromatin)
GAPDH
WDR13
p53
TBP
C
p53
p21
mRNA expression level
P =0.0045
P =0.0033
D
WT
ΔCoTC
UV
p53
p21
HSP90
E
WT
ΔCoTC
(-UV)
(+UV)
G0-G1
S phase
G2-M
45,8
12,7
19,2
45,1
12,0
20,7
46,7
15,2
16,5
29,4
16,3
27,8
Count
PI

Figure 4.

Figure 4. The CoTC is implicated in the maintenance of 3′-end processing of *p53* pre-mRNA in response to UV-induced DNA damage.

A RT–qPCR assay on nuclear RNA for assessing the uncleaved/total ratio of *p53* pre-mRNA in wild type (WT) and CoTC-deleted (ΔCoTC) A549 cells ($n = 3$) treated with or without UV irradiation (40 J/m^2).

B RT–qPCR analysis on RNA extracted from nucleoplasm and chromatin fractions. The ratio of uncleaved pre-mRNA (nucleoplasm/chromatin) was calculated to quantify the level of unprocessed *p53*, *WDR13*, *GAPDH*, and *TBP* pre-mRNA ($n = 3$) released in the nucleoplasm compared with the chromatin-bound unprocessed pre-mRNA in wild type (WT) and CoTC-deleted (ΔCoTC) A549 cells treated with or without UV irradiation (40 J/m^2).

C RT–qPCR measuring relative *p53* and *p21* mRNA levels in wild type (WT) and CoTC-deleted (ΔCoTC) cells ($n = 3$) in response to UV treatment (40 J/m^2). The expression was normalized to HPRT.

D Western blot analysis of p53 and p21 expression in wild type (WT) and CoTC-deleted (ΔCoTC) A549 cells ($n = 3$) treated with or without UV irradiation (40 J/m^2).

E Representative flow-cytometry analyses of the cell cycle (DNA content by Propidium Iodide; PI) in wild type (WT) and CoTC-deleted (ΔCoTC) A549 cells ($n = 3$) treated with or without UV irradiation (40 J/m^2). Indicated: percent of cells in the G0-G1, S, and G2/M phases.

Data information: "*n*" indicates the number of biological replicates for each experiment. All data are presented as the mean ± s.e.m. *P*-values were calculated using a two-sided unpaired *t*-test.

Source data are available online for this figure.

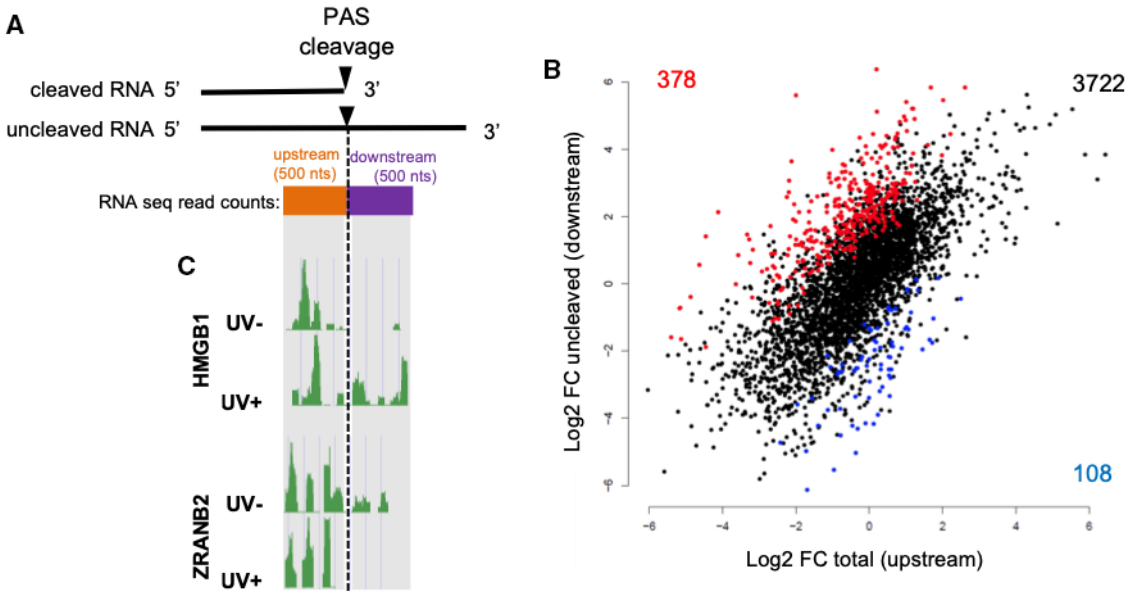

Figure 5. UV induces widespread regulation of pre-mRNA 3′-end processing.

A Scheme representing the adopted strategy to study at genome wide level by RNA-sequencing the regulation of pre-mRNA 3′-end processing in response to UV. Nuclear RNA from A549 cells UV-irradiated or -unirradiated was extracted and cDNA library preparation was performed to assess RNA-sequencing. The efficiency of 3′-end processing was studied by the quantification of the number of reads located in a window of 500 bp downstream (uncleaved RNA) and upstream (total RNA) of the poly (A) site. The ratio of reads downstream / reads upstream reflects the efficiency of pre-mRNA 3′-end processing.

B RNA-seq plot representing, for each gene, the log2 fold change (comparing UV-irradiated to nonirradiated cells) of the number of reads downstream of the poly(A) site (uncleaved RNA, *y* axis), and the log2 fold change of the number of reads upstream of the poly(A) site (total RNA, *x* axis; $n = 3$). Regulation events are considered significant if *P*-value is below 0.05. The 108 genes at bottom right have a decreased uncleaved/total RNA ratio, meaning that PAS cleavage is increased upon UV irradiation. By contrast, the 378 genes at top left have an increased uncleaved/total RNA ratio, meaning that PAS cleavage is decreased upon UV irradiation.

C Visualization of reads distribution in a window of 500 nts upstream and downstream of the PAS of *HMGB1* and *ZRANB2* pre-mRNA.

transcriptional PAS cleavage that is nucleoplasmic and PCF11-independent and occurs following a CoTC-dependent release of the pre-mRNA from chromatin. Our model thus explains the rescue of the 3′-end processing of specific mRNAs in a transcription-uncoupled manner, despite the global inhibition by UV-induced DNA damage of the canonical chromatin-associated pre-mRNA

Figure 6. The 3′-end processing of diverse pre-mRNAs undergoing a CoTC cleavage event is maintained in response to UV-induced DNA damage.

A RT–qPCR (uncleaved/total RNA) on nuclear RNA extracted from UV-treated or -untreated A549 cells ($n = 3$), to assess the regulation of 3′-end processing of 20 pre-mRNAs randomly selected from the previous RNA-sequencing data.

B RT–qPCR (Released uncleaved pre-mRNA nucleoplasm/chromatin) on RNA extracted from the nucleoplasm and the chromatin fractions of A549 UV-treated cells ($n = 3$).

Data information: "*n*" indicates the number of biological replicates for each experiment. All data are presented as the mean ± s.e.m.
Source data are available online for this figure.

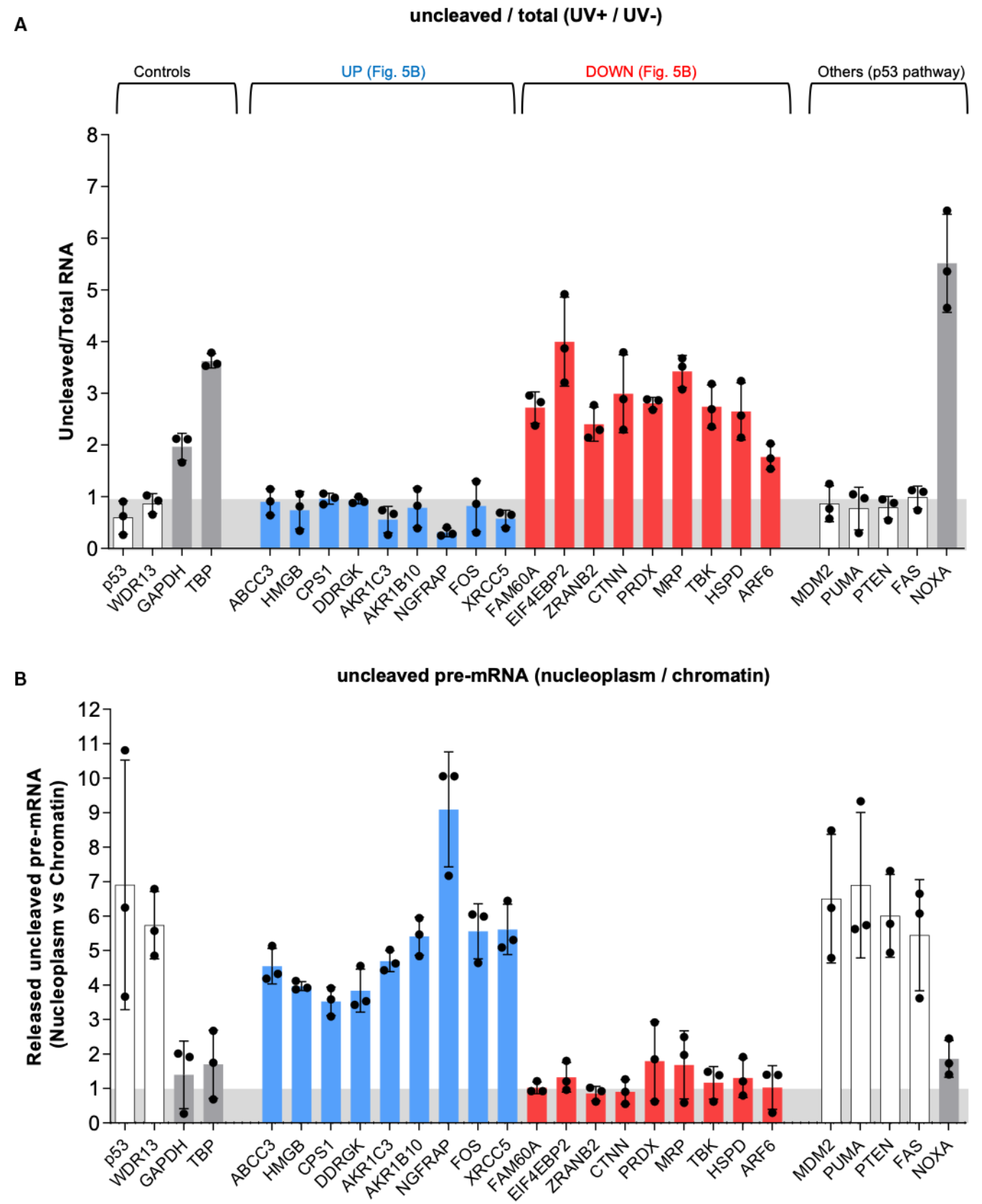

Figure 6.

processing that is tightly coordinated to transcriptional termination (Luna *et al*, 2005; Hamperl *et al*, 2017; Nilsson *et al*, 2018; Teloni *et al*, 2019; Reimer *et al*, 2021). Nucleoplasmic PAS-dependent 3′ cleavage occurs following a CoTC-dependent release of the pre-mRNA, thereby acting as a compensatory mechanism to maintain the expression of genes involved in the p53 pathway and DNA damage response.

Materials and Methods

Cell culture, siRNA transfections, and UV irradiation

A549 cells were cultured in DMEM (Eurobio) containing 10% FCS (Pan Biotech) and L-Glutamine (Eurobio) at 37°C in 5% CO_2. siRNA reverse transfections were performed in 10 cm with Lipofectamine RNAiMAX (Thermo Scientific) at a final concentration of 20 nM siRNA (Eurogentec or Dharmacon; see Appendix Table S1) as per the manufacturer's instructions in OptiMEM reduced serum media (Thermo Scientific). After 48 h transfection, cells were washed with PBS and irradiated with 40 J/m^2 UV (254 nm; Stratalinker), placed in fresh media, and harvested on ice after 16 h of recovery at 37°C.

CRISPR-mediated deletion of CoTC element

CRISPR sgRNAs were designed for the CoTC element deletion of the p53 gene (Appendix Fig S2). sgRNAs were designed using the online tool http://crispr.mit.edu/. Guide sequences are identified that minimize identical genomic matches or near-matches to reduce the risk of cleavage away from target sites (off-target effects). The guide sequences are constructed such that they consist of 20-mer protospacer sequence upstream of an NGG protospacer adjacent motif (PAM) at the genomic recognition site (Appendix Table S2).

Two sgRNA oligos are constructed, each of 24–25 mer oligos and their associated reverse complement including additional nucleotides for cloning and expression purposes.

The two plasmids used are namely, pSpCas9 (BB) plasmid pX458 and pX459, which include GFP and puromycin as selectable markers, respectively.

i First the sequences CACC and AAAC are added before the 20-mer guide sequence and the guide's reverse complement for cloning into pX458/pX459 vectors using BbsI restriction enzyme (Appendix Table S3).
ii A G nucleotide is added after the CACC sequence and before the 20-mer if the first position of the 20-mer is not G. sgRNA expression from the U6 promoter of the pX458/pX459 vector is enhanced by the inclusion of a G nucleotide after the CACC sequence.
iii A C nucleotide is added at the 3′-end of the reverse complement oligo. All resultant oligos are 25-mer oligos.

The sgRNA oligo sequences were cloned into the pX458 and pX459 plasmids using a Golden Gate assembly cloning strategy (Appendix Fig S3B). The plasmids were amplified followed by transfection. Selection of transfected cells was carried out in puromycin-containing medium. The cells are incubated for a total of 48–72 h after transfection before harvesting for indel analysis.

Primers were designed surrounding the sgRNA cleavage sites for PCR and screening for CRISPR/Cas9 screening deletion (Appendix Fig S3). gDNA was isolated from control or transfected cells, and PCR is performed to validate the primers and verify the presence of the intended genomic deletion.

Cell fractionation

Cell pellets were resuspended in approximately 3× cell pellet volume of lysis Buffer A (10 mM HEPES pH 7.9, 15 mM $MgCl_2$, 10 mM KCl, 0.1% NP40, 1 mM DTT) containing RNAseOut (Thermo Scientific) and incubated on ice for 15 min. Cells were then pelleted at 1,000 *g* for 5 min at 4°C and the supernatant retained for cytoplasmic RNA. Nuclear pellets were washed in 2 × 1 ml Lysis Buffer A at 1,000 *g* for 5 min at 4°C, resuspended in 2 × pellet volume with Nuclear Lysis Buffer B (20 mM HEPES pH 7.9, 400 mM NaCl, 1.5 M $MgCl_2$, 0.2 mM EDTA, 5 mM DTT) containing RNAseOut and incubated on ice for 30 min. Nuclear debris was pelleted at 10,000 *g* for 15 min at 4°C, and supernatants were placed in Trizol Reagent for RNA extraction.

Nuclear fractionation

Cell nuclei were suspended in 1× nuclei pellet volume of buffer 1 (20 mM Tris–pH 7.9, 75 mM NaCl, 0.5 mM EDTA, 0.85 mM DTT, 0.125 mM PMSF, 0.1 mg of yeast tRNA/ml, 50% glycerol) and 10× nuclei pellet volume of buffer 2 (20 mM HEPES, 300 mM NaCl, 1 mM DTT, 7.5 mM MgCl2, 0.2 mM EDTA, 1 M Urea, 1% NP-40, 0.1 mg of yeast tRNA/ml). After vigorous agitation for 5 s, nuclei pellet was incubated for 10 min on ice. Chromatin fraction was then sedimented by full-speed centrifugation for 5 min at 4°C. The supernatant corresponding to the nucleoplasmic fraction was transferred to a new tube, adjusted to 0.1% of SDS, and trizol RNA extraction was proceeded. The insoluble fraction corresponding to the chromatin was resuspended in buffer 3 (10 mM Tris–pH 7.5, 10 mM MgCl2, 500 mM NaCl), and 20 U of DNAse was added before 30 min incubation at 37°C. RNA extraction was then proceeded.

RT–qPCR and RT–PCR

cDNA was synthesized using Superscript III (Thermo Scientific). qPCR on cDNA derived from nuclear pre-mRNAs or cytoplasmic mRNAs was performed using 2× Power Sybrgreen Master Mix (Thermo Scientific) and 0.4 μM oligonucleotide primers (Appendix Table S4). The ratio of uncleaved/total RNA was calculated using $2^{(\text{total-uncleaved})}$, and the ratio of released uncleaved RNA nucleoplasm/ chromatin-associated uncleaved pre-mRNA was calculated using $2^{(\text{Chromatin-nucleoplasm})}$. For the RNA-IP, samples were normalized to the input using $2^{(\text{Input-IP})}$. When conducting RT–PCR, cDNA amplification was performed using Go-Taq flexi DNA polymerase (Promega). PCR products were then applied to 1% agarose gel.

Western blot

Cells were harvested on ice and pelleted by centrifugation at 400 *g* for 5 min at 4°C. Pellets were resuspended in RIPA Buffer containing complete protease inhibitors (EDTA-free) and sonicated (Bioruptor,

Diagenode). Cellular debris was pelleted at 11,000 *g* for 10 min at 4°C and protein concentration determined. Primary antibodies used in this study from Bethyl Laboratories were: CPSF160, CPSF100, CPSF73, CPSF30, CstF77, CstF64, CstF50, CFIm68, and CFIm59. Other antibodies used include CFIm25 (PTGlabs), PCF11 (Santa-Cruz), and CLP1 (Epitomics). GAPDH (Sigma), Ser2P (Millipore), Topoisomerase II α (Abcam), Histone H3 (Abcam), DHX36 (Abcam), hnRNP (H/F; Abcam), p21 (Thermofisher), and p53 (Cell Signaling Technology).

Single-molecule fluorescence *in situ* hybridization (FISH)

A549 cells were cultured on #1.5 cover glasses in 12-well plates. When cells were at approximately 50% confluency, the cover glass was washed once with PBS. Each cover glass was placed in one well of a 12-well plate that was filled with 200 µl PBS, which just barely covered the top of the cover glass. Half of the cover glasses were irradiated with UVC at 50 J/m^2. After irradiation, cover glasses were returned to the culture medium and placed in the incubator for 4 h. After 4 h, cells on cover glasses were washed 3 times with HBSS before fixation with 4% PFA in PBS. Fixed samples were washed with 1× PBS and stored in 70% ethanol at 4°C overnight.

FISH probes were designed and ordered from Biosearch Stellaris using Quasar 570 and 670 fluorophores. Hybridizations were performed according to the manufacturer's protocol with minor modifications. Hybridized samples were mounted in Prolong Gold with DAPI and allowed to dry overnight.

Imaging of FISH was performed on a custom-built microscope. This microscope comprised an ASI (www.asiimaging.com) Rapid Automated Modular Microscope System (RAMM) base, a Hamamatsu ORCA-Flash4 V2 CMOS camera (https://www.hamamatsu.com/, C11440), Lumencore SpectraX (https://lumencor.com/), an ASI High Speed Filter Wheel (FW-1000), and an ASI MS-2000 Small XY stage. Excitation of DAPI, Quasar 570, and 670 was performed using SpectraX violet, red, and green, respectively. Emission filters specific to these spectra were used. Image acquisition was performed through Micro-Manager. We obtained multiple z stacks at 250 ms exposures, 0.5 µm intervals, spanning 3.5 µm. The maximum intensity projections were performed and used for transcript localization and analysis.

FISH analysis was performed with custom MATLAB software. Briefly, images of cells were segmented into the nucleus and cytoplasm. Spots were localized with custom MATLAB software using an algorithm based on Thompson et al. The software outputs the number of nuclear and cytoplasmic spots per cell, and the distribution of spots per cell (Appendix Fig S11).

Propidium iodide staining

Cells were harvested in ice and washed with PBS. They were fixed in 70% ethanol for 30 min at −20°C. They were washed twice in PBS pelleted by centrifugation at 850 *g* for 5 min at 4°C. The cells were then resuspended in a solution containing 3.5 mM Tris–HCl pH 7.6 (Thermo Scientific), 10 mM NaCl (Thermo Scientific), 50 µg/ml propidium iodide (Sigma P4170), 0.1% IGEPAL (Thermo Scientific), 20 µg/ml RnaseA (Sigma), and water. The acquisition of stained cells was performed using an LSRII flow cytometer (BD Biosciences). The acquired data were analyzed using FlowJo software.

RNA-sequencing analysis

For RNA-seq, nuclear RNA from UV-irradiated and nonirradiated A549 cells (two biological replicates of each condition) was subjected to DNAse I treatment with TURBO DNase I (ThermoFisher Scientific), quantified, and analyzed using an RNA 2100 Bioanalyzer (Agilent). 500 ng of good quality RNA (RIN > 9) was used for Illumina compatible library preparation using the TruSeq Stranded total RNA protocol allowing to take into account strand information. A first step of ribosomal RNA depletion was performed using the Ribo-Zero Gold kit (Illumina). After fragmentation, cDNA synthesis was performed and resulting fragments were used for dA-tailing followed by ligation of TruSeq indexed adapters. PCR amplification was finally achieved to generate the final barcoded cDNA libraries. Libraries were equimolarly pooled. Sequencing was carried out on a HiSeq instrument (Illumina) to obtain around 40 million raw single-end reads of 100 nucleotides per sample.

Fastq files were generated using bcl2fastq. RNA-seq reads of good quality were trimmed in their 5′- and 3′-ends with the cutadapt software to remove uninformative nucleotides due to primer sequences. Trimmed reads of 100 bp or more were aligned on the Human genome (hg19) using Tophat2. Only reads with a mapping quality score of 20 or more were retained (samtools) for downstream analysis. Gene coordinates were obtained on the basis of overlapping Refseq transcripts with the same gene symbol. For each gene, two 500 bp regions located upstream and downstream of the PAS at the end of the gene were defined (genes with a downstream region overlapping another gene were discarded), and reads located in the upstream and downstream regions were counted in each sample. A table of counts was built with the featureCounts software (R version 3.4.0). Only genes with at least 10 reads in both regions in either condition were kept for further analysis. In total, 4,208 genes passed all these steps and were used for subsequent analysis. The differential analysis between the UV+ and UV− conditions was done using two independent biological replicates per condition. For each gene, the fold regulation of the downstream region (that is the ratio of normalized read counts between conditions) was compared with the fold regulation of the upstream region using a Wald test implemented in DESeq2 (Love *et al*, 2014).

Gene ontology (GO) analysis of genes was carried out by the functional enrichment analysis tool DAVID.

Statistics

Statistical differences between experimental and control samples were assessed by the unpaired *t*-test using GraphPad Prism, with significance achieved at $P < 0.05$.

Data availability

The datasets produced in this study are available in the following databases: Gene Expression Omnibus repository (GEO) under accession number GSE203517 (https://www.ncbi.nlm.nih.gov/geo/query/acc.cgi?acc=GSE203517). All other data generated or analyzed during this study are included in the manuscript.

Expanded View for this article is available online.

Acknowledgements

We thank the Institut Curie Next Generation Sequencing platform (Sylvain Baulande) for high-throughput sequencing. Research was funded by grants from Equipe labellisée Ligue Nationale Contre le Cancer (LNCC), Institut Curie, Gustave Roussy, and Centre National de la Recherche Scientifique (CNRS). R.S. was successively supported by a predoctoral fellowship from the Ministère de l'Enseignement Supérieur et de la Recherche (MESR) and the Association pour la Recherche sur le Cancer (ARC).

Author contributions

Rym Sfaxi: Formal analysis; investigation; methodology; writing – original draft; writing – review and editing. **Biswendu Biswas:** Formal analysis; investigation; methodology; writing – original draft; writing – review and editing. **Galina Boldina:** Formal analysis; investigation; methodology. **Mandy Cadix:** Software; formal analysis. **Nicolas Servant:** Software; formal analysis. **Huimin Chen:** Investigation; methodology. **Daniel R Larson:** Conceptualization; formal analysis; investigation. **Martin Dutertre:** Conceptualization; writing – review and editing. **Caroline Robert:** Formal analysis; supervision; funding acquisition; writing – review and editing. **Stéphan Vagner:** Conceptualization; formal analysis; supervision; funding acquisition; investigation; methodology; writing – original draft; writing – review and editing.

Disclosure and competing interests statement

SV is a shareholder and founder of Ribonexus. CR is a shareholder and founder of Ribonexus and an occasional consultant for Roche, BMS, MSD, Merck, Sanofi, Pierre Fabre, Biothera, CureVac, and Novartis. The other authors declare that they have no conflict of interest.

References

Ahn SH, Kim M, Buratowski S (2004) Phosphorylation of serine 2 within the RNA polymerase II C-terminal domain couples transcription and 3′ end processing. *Mol Cell* 13: 67 – 76

Barilla D, Lee BA, Proudfoot NJ (2001) Cleavage/polyadenylation factor IA associates with the carboxyl-terminal domain of RNA polymerase II in Saccharomyces cerevisiae. *Proc Natl Acad Sci U S A* 98: 445 – 450

Blackford AN, Jackson SP (2017) ATM, ATR, and DNA-PK: the trinity at the heart of the DNA damage response. *Mol Cell* 66: 801 – 817

Céraline J, Deplanque G, Duclos B, Limacher J-M, Hajri A, Noel F, Orvain C, Frébourg T, Klein-Soyer C, Bergerat J-P (1998) Inactivation of p53 in normal human cells increases G2/M arrest and sensitivity to DNA-damaging agents. *Int J Cancer* 75: 432 – 438

Cortazar MA, Sheridan RM, Erickson B, Fong N, Glover-Cutter K, Brannan K, Bentley DL (2019) Control of RNA pol II speed by PNUTS-PP1 and Spt5 dephosphorylation facilitates termination by a "sitting duck torpedo" mechanism. *Mol Cell* 76: 896 – 908

Decorsière A, Cayrel A, Vagner S, Millevoi S (2011) Essential role for the interaction between hnRNP H/F and a G quadruplex in maintaining p53 pre-mRNA 3′-end processing and function during DNA damage. *Genes Dev* 25: 220 – 225

Dye MJ, Proudfoot NJ (2001) Multiple transcript cleavage precedes polymerase release in termination by RNA polymerase II. *Cell* 105: 669 – 681

Eaton JD, Davidson L, Bauer DLV, Natsume T, Kanemaki MT, West S (2018) Xrn2 accelerates termination by RNA polymerase II, which is underpinned by CPSF73 activity. *Genes Dev* 32: 127 – 139

Galanos P, Vougas K, Walter D, Polyzos A, Maya-Mendoza A, Haagensen EJ, Kokkalis A, Roumelioti F-M, Gagos S, Tzetis M *et al* (2016) Chronic p53-independent p21 expression causes genomic instability by deregulating replication licensing. *Nat Cell Biol* 18: 777 – 789

Gromak N, West S, Proudfoot NJ (2006) Pause sites promote transcriptional termination of mammalian RNA polymerase II. *Mol Cell Biol* 26: 3986 – 3996

Grzechnik P, Gdula MR, Proudfoot NJ (2015) Pcf11 orchestrates transcription termination pathways in yeast. *Genes Dev* 29: 849 – 861

Hamperl S, Bocek MJ, Saldivar JC, Swigut T, Cimprich KA (2017) Transcription-replication conflict orientation modulates R-loop levels and activates distinct DNA damage responses. *Cell* 170: 774 – 786

Jeong J-H, Kang S-S, Park K-K, Chang H-W, Magae J, Chang Y-C (2010) p53-independent induction of G_1 arrest and $p21^{WAF1/CIP1}$ expression by Ascofuranone, an isoprenoid antibiotic, through downregulation of c-Myc. *Mol Cancer Ther* 9: 2102 – 2113

Kamieniarz-Gdula K, Gdula MR, Panser K, Nojima T, Monks J, Wiśniewski JR, Riepsaame J, Brockdorff N, Pauli A, Proudfoot NJ (2019) Selective roles of vertebrate PCF11 in premature and full-length transcript termination. *Mol Cell* 74: 158 – 172

Kim H-S, Li H, Cevher M, Parmelee A, Fonseca D, Kleiman FE, Lee SB (2006) DNA damage-induced BARD1 phosphorylation is critical for the inhibition of messenger RNA processing by BRCA1/BARD1 complex. *Cancer Res* 66: 4561 – 4565

Kleiman FE (1999) Functional interaction of BRCA1-associated BARD1 with polyadenylation factor CstF-50. *Science* 285: 1576 – 1579

Kleiman FE, Manley JL (2001) The BARD1-CstF-50 interaction links mRNA 3′ end formation to DNA damage and tumor suppression. *Cell* 104: 743 – 753

Larochelle M, Robert M-A, Hébert J-N, Liu X, Matteau D, Rodrigue S, Tian B, Jacques P-É, Bachand F (2018) Common mechanism of transcription termination at coding and noncoding RNA genes in fission yeast. *Nat Commun* 9: 4364

Latonen L, Taya Y, Laiho M (2001) UV-radiation induces dose-dependent regulation of p53 response and modulates p53-HDM2 interaction in human fibroblasts. *Oncogene* 20: 6784 – 6793

Licatalosi DD, Geiger G, Minet M, Schroeder S, Cilli K, McNeil JB, Bentley DL (2002) Functional interaction of yeast pre-mRNA 3′ end processing factors with RNA polymerase II. *Mol Cell* 9: 1101 – 1111

Love MI, Huber W, Anders S (2014) Moderated estimation of fold change and dispersion for RNA-seq data with DESeq2. *Genome Biol* 15: 550

Luna R, Jimeno S, Marín M, Huertas P, García-Rubio M, Aguilera A (2005) Interdependence between transcription and mRNP processing and export, and its impact on genetic stability. *Mol Cell* 18: 711 – 722

Luo W (2006) The role of Rat1 in coupling mRNA 3′-end processing to transcription termination: implications for a unified allosteric-torpedo model. *Genes Dev* 20: 954 – 965

Masamha CP, Xia Z, Yang J, Albrecht TR, Li M, Shyu A-B, Li W, Wagner EJ (2014) CFIm25 links alternative polyadenylation to glioblastoma tumour suppression. *Nature* 510: 412 – 416

Matsuda T, Kato T, Kiyotani K, Tarhan YE, Saloura V, Chung S, Ueda K, Nakamura Y, Park J-H (2017) p53-independent p21 induction by MELK inhibition. *Oncotarget* 8: 57938 – 57947

Meinhart A, Cramer P (2004) Recognition of RNA polymerase II carboxy-terminal domain by 3′-RNA-processing factors. *Nature* 430: 223 – 226

Millevoi S, Vagner S (2010) Molecular mechanisms of eukaryotic pre-mRNA 3′ end processing regulation. *Nucleic Acids Res* 38: 2757 – 2774

Muñoz MJ, Santangelo MSP, Paronetto MP, de la Mata M, Pelisch F, Boireau S, Glover-Cutter K, Ben-Dov C, Blaustein M, Lozano JJ *et al* (2009) DNA damage regulates alternative splicing through inhibition of RNA polymerase II elongation. *Cell* 137: 708 – 720

Nazeer FI, Devany E, Mohammed S, Fonseca D, Akukwe B, Taveras C, Kleiman FE (2011) p53 inhibits mRNA 3′ processing through its interaction with the CstF/BARD1 complex. *Oncogene* 30: 3073 – 3083

Newman M, Sfaxi R, Saha A, Monchaud D, Teulade-Fichou M-P, Vagner S (2017) The G-quadruplex-specific RNA helicase DHX36 regulates p53 pre-mRNA 3′-end processing following UV-induced DNA damage. *J Mol Biol* 429: 3121 – 3131

Nilsson K, Wu C, Kajitani N, Yu H, Tsimtsirakis E, Gong L, Winquist EB, Glahder J, Ekblad L, Wennerberg J *et al* (2018) The DNA damage response activates HPV16 late gene expression at the level of RNA processing. *Nucleic Acids Res* 46: 5029 – 5049

Nojima T, Dienstbier M, Murphy S, Proudfoot NJ, Dye MJ (2013) Definition of RNA polymerase II CoTC terminator elements in the human genome. *Cell Rep* 3: 1080 – 1092

Nourse J, Spada S, Danckwardt S (2020) Emerging roles of RNA 3′-end cleavage and polyadenylation in pathogenesis, diagnosis and therapy of human disorders. *Biomolecules* 10: 915

Ogorodnikov A, Levin M, Tattikota S, Tokalov S, Hoque M, Scherzinger D, Marini F, Poetsch A, Binder H, Macher-Göppinger S *et al* (2018) Transcriptome 3'end organization by PCF11 links alternative polyadenylation to formation and neuronal differentiation of neuroblastoma. *Nat Commun* 9: 5331

van Oosten M, Rebel H, Friedberg EC, van Steeg H, van der Horst GTJ, van Kranen HJ, Westerman A, van Zeeland AA, Mullenders LHF, de Gruijl FR (2000) Differential role of transcription-coupled repair in UVB-induced G2 arrest and apoptosis in mouse epidermis. *Proc Natl Acad Sci U S A* 97: 11268 – 11273

Pavey S, Russell T, Gabrielli B (2001) G2 phase cell cycle arrest in human skin following UV irradiation. *Oncogene* 20: 6103 – 6110

Proudfoot NJ (2016) Transcriptional termination in mammals: stopping the RNA polymerase II juggernaut. *Science* 352: aad9926

Reimer KA, Mimoso CA, Adelman K, Neugebauer KM (2021) Co-transcriptional splicing regulates 3′ end cleavage during mammalian erythropoiesis. *Mol Cell* 81: 998 – 1012

Rockx DA, Mason R, van Hoffen A, Barton MC, Citterio E, Bregman DB, van Zeeland AA, Vrieling H, Mullenders LH (2000) UV-induced inhibition of transcription involves repression of transcription initiation and phosphorylation of RNA polymerase II. *Proc Natl Acad Sci U S A* 97: 10503 – 10508

Shi Y, Manley JL (2015) The end of the message: multiple protein–RNA interactions define the mRNA polyadenylation site. *Genes Dev* 29: 889 – 897

Shi Y, Di Giammartino DC, Taylor D, Sarkeshik A, Rice WJ, Yates JR, Frank J, Manley JL (2009) Molecular architecture of the human pre-mRNA 3′ processing complex. *Mol Cell* 33: 365 – 376

Sikes M, Beyer A, Osheim Y (2002) EM visualization of pol II genes in drosophila: most genes terminate without prior 3′ end cleavage of nascent transcripts. *Chromosoma* 111: 1 – 12

Teixeira A, Tahiri-Alaoui A, West S, Thomas B, Ramadass A, Martianov I, Dye M, James W, Proudfoot NJ, Akoulitchev A (2004) Autocatalytic RNA cleavage in the human beta-globin pre-mRNA promotes transcription termination. *Nature* 432: 526 – 530

Teloni F, Michelena J, Lezaja A, Kilic S, Ambrosi C, Menon S, Dobrovolna J, Imhof R, Janscak P, Baubec T *et al* (2019) Efficient pre-mRNA cleavage prevents replication-stress-associated genome instability. *Mol Cell* 73: 670 – 683

Vilborg A, Passarelli MC, Yario TA, Tycowski KT, Steitz JA (2015) Widespread inducible transcription downstream of human genes. *Mol Cell* 59: 449 – 461

Wang R, Zheng D, Wei L, Ding Q, Tian B (2019) Regulation of intronic polyadenylation by PCF11 impacts mRNA expression of long genes. *Cell Rep* 26: 2766 – 2778

West S, Proudfoot NJ (2007) Human Pcf11 enhances degradation of RNA polymerase II-associated nascent RNA and transcriptional termination. *Nucleic Acids Res* 36: 905 – 914

West S, Proudfoot NJ, Dye MJ (2008) Molecular dissection of mammalian RNA polymerase II transcriptional termination. *Mol Cell* 29: 600 – 610

White E, Kamieniarz-Gdula K, Dye MJ, Proudfoot NJ (2013) AT-rich sequence elements promote nascent transcript cleavage leading to RNA polymerase II termination. *Nucleic Acids Res* 41: 1797 – 1806

Zhang Y, Liu L, Qiu Q, Zhou Q, Ding J, Lu Y, Liu P (2021) Alternative polyadenylation: methods, mechanism, function, and role in cancer. *J Exp Clin Cancer Res* 40: 51

Expanded View Figures

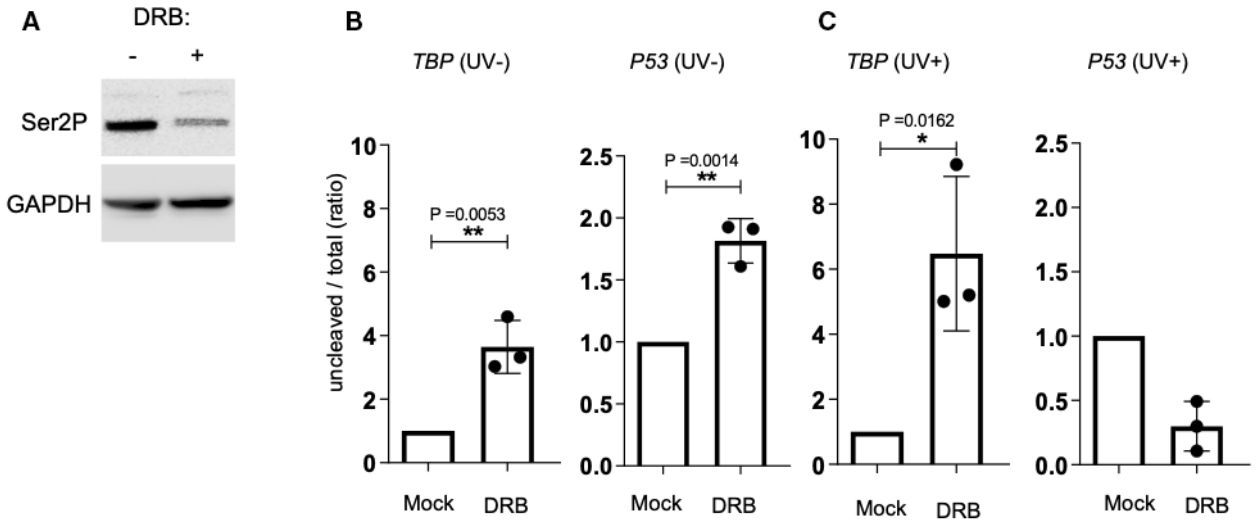

Figure EV1. The Pol II Ser^2 kinase (CDK9) inhibitor DRB has no impact on *p53* 3′-end processing in UV-treated cells.

A Western Blot analysis of the CTD phospho-Ser2 expression in A549 cells treated with DRB (50 μM) for 24 h prior to UV irradiation (40 J/m^2; $n = 3$).

B RT–qPCR to assess the efficiency of p53 and TBP pre-mRNA 3′-end processing in A549 cells ($n = 3$) treated with DRB (50 μM) for 24 h without UV treatment.

C RT–qPCR to assess the efficiency of p53 and TBP pre-mRNA 3′-end processing in A549 cells ($n = 3$) treated with DRB (50 μM) for 24 h prior to UV irradiation (40 J/m^2)

Data information: "*n*" indicates the number of biological replicates for each experiment. All data are presented as the mean ± s.e.m. *P*-values were calculated using a two-sided unpaired *t*-test.
Source data are available online for this figure.

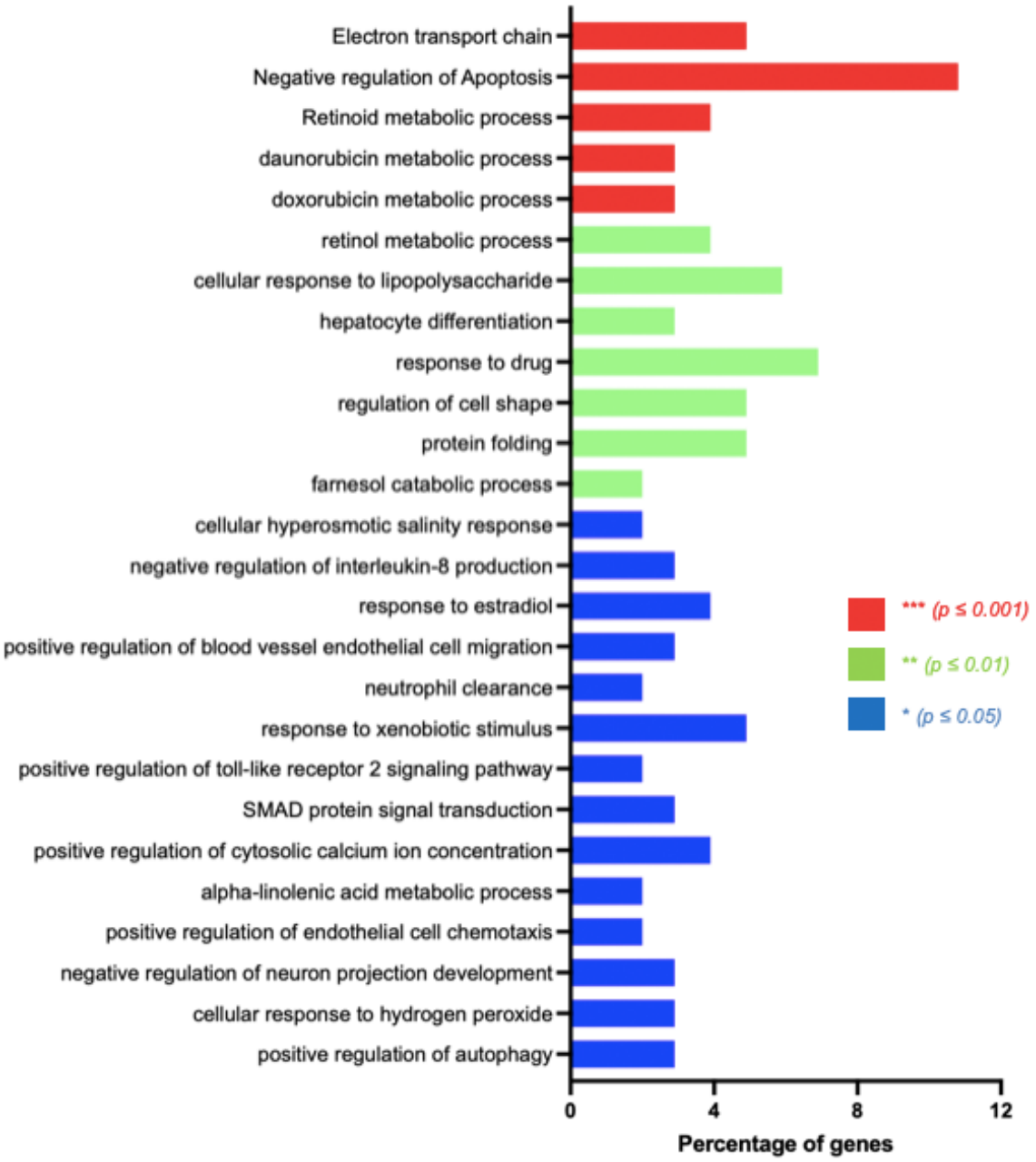

Figure EV2. Gene ontology (GO) analysis of the 108 pre-mRNAs with a more efficient 3′-end processing in UV-treated compared with untreated cells.

Data are obtained from RNA-sequencing analyses. The bar chart shows the GO terms for biological processes, ranked by *P*-values, calculated by the functional enrichment analysis tool DAVID.

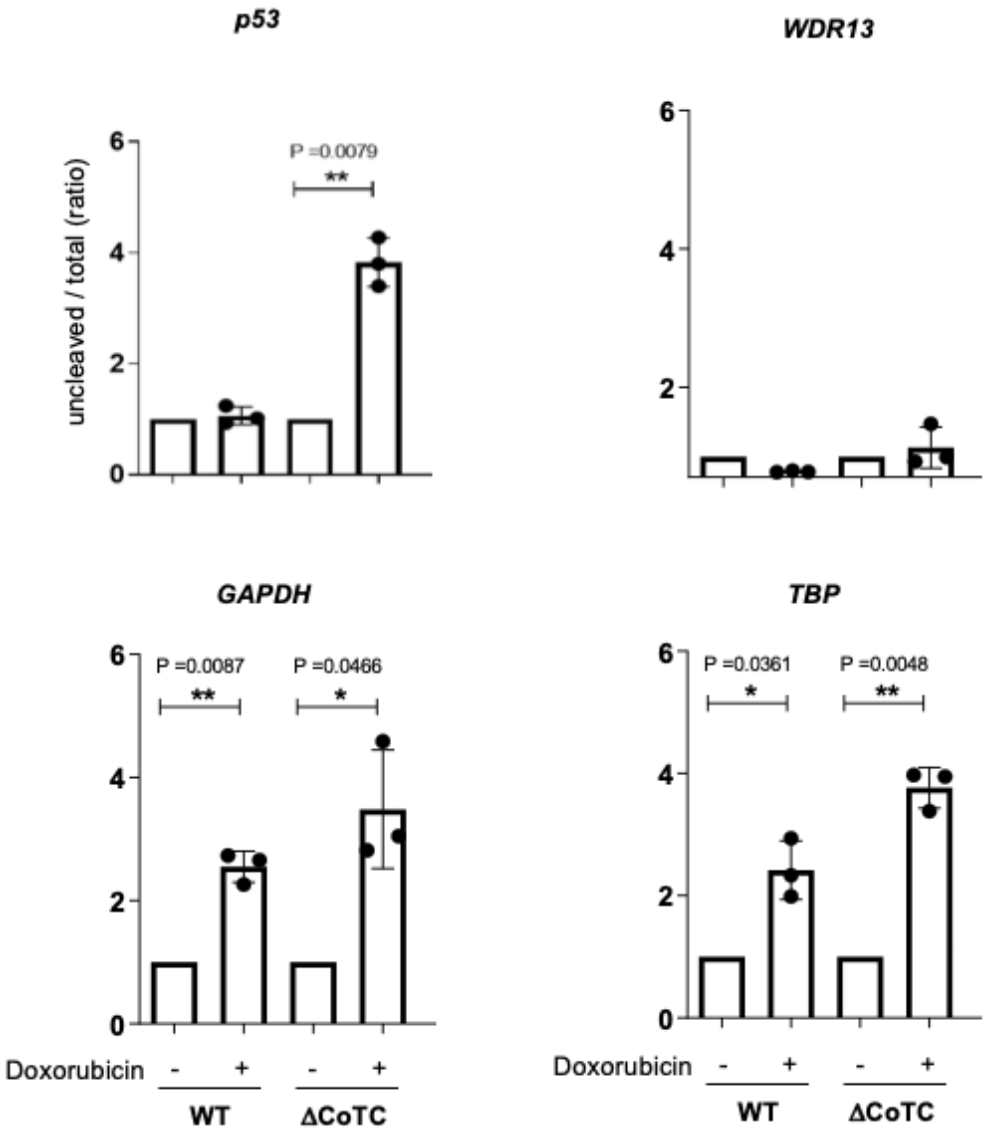

Figure EV3. The *p53* CoTC region is required for the maintenance of *p53* pre-mRNA 3′-end processing upon doxorubicin treatment.

RT–qPCR assay on nuclear RNA for assessing the uncleaved/total ratio of *p53* pre-mRNA in wild type (WT) and CoTC-deleted (ΔCoTC) A549 cells treated with or without doxorubicin (3.5 μM). ($n = 3$); *P*-values were calculated using a two-sided unpaired *t*-test.

Source data are available online for this figure.

APPENDIX

Uncoupling from transcription protects polyadenylation site cleavage from inhibition by DNA damage

Rym Sfaxi[1,2,3,#], Biswendu Biswas[1,2,3,4,5,#], Galina Boldina[1,2,3], Mandy Cadix[1,2,3], Nicolas Servant[6], Huimin Chen[7], Daniel R. Larson[7], Martin Dutertre[1,2,3], Caroline Robert[4,5], Stéphan Vagner[1,2,3,*]

[1]Institut Curie, PSL Research University, CNRS UMR3348, INSERM U1278, F-91405, Orsay, France ;
[2]Université Paris Sud, Université Paris-Saclay, CNRS UMR3348, INSERM U1278, F-91405 Orsay, France ;
[3]Equipe Labellisée Ligue Contre le Cancer;
[4]INSERM U981, Gustave Roussy, Villejuif, France;
[5]Université Paris Sud, Université Paris-Saclay, Kremlin-Bicêtre, France.
[6]INSERM U900, Institut Curie, PSL Research University, Mines ParisTech, 26 rue d'Ulm, 75005, Paris, France ;
[7]Laboratory of Receptor Biology and Gene Expression, National Cancer Institute, NIH, Bethesda, MD 20892, USA

[#]Joint first authors
[*]Corresponding author: Stephan.Vagner@curie.fr

Table of contents

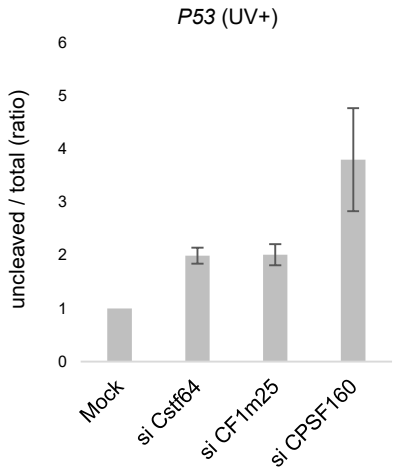

Appendix Figure S1. ***siRNA-mediated depletion of CstF64, CFIm25 and CPSF160 inhibits p53 PAS cleavage in response to UV.*** RT-qPCR assay on nuclear RNA for assessing the uncleaved/total ratio of *p53* pre-mRNA in A549 cells transfected for 48 hours with siRNAs targeting the Cstf64, CF1m25 and CPSF160 and exposed to UV irradiation (40 J/m2) (n=3 technical replicates).

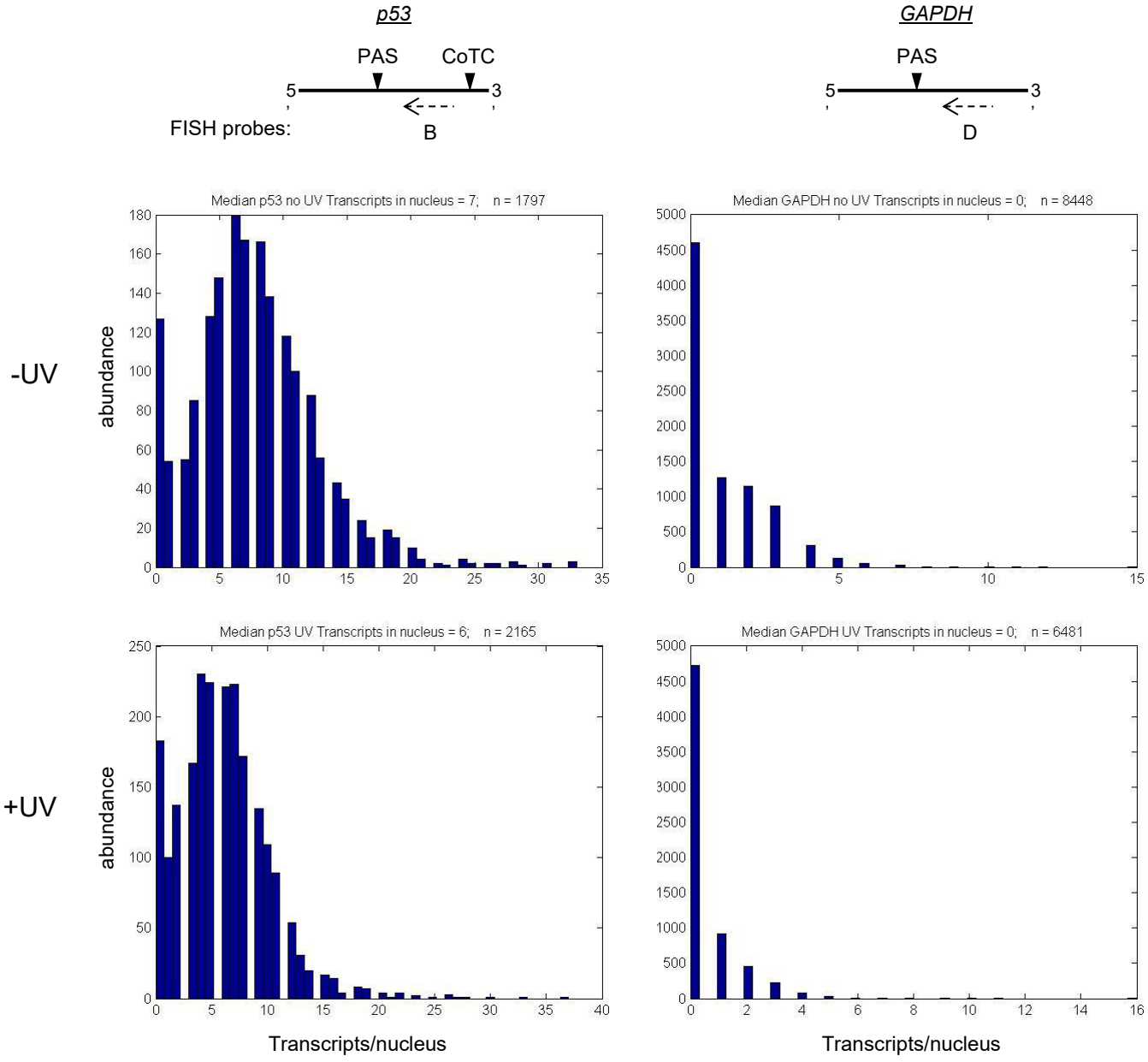

Appendix Figure S2. ***Distribution of spots per cell in the smFISH experiments.*** Distribution of spots per cell in the smFISH experiments (related to Figure 3).

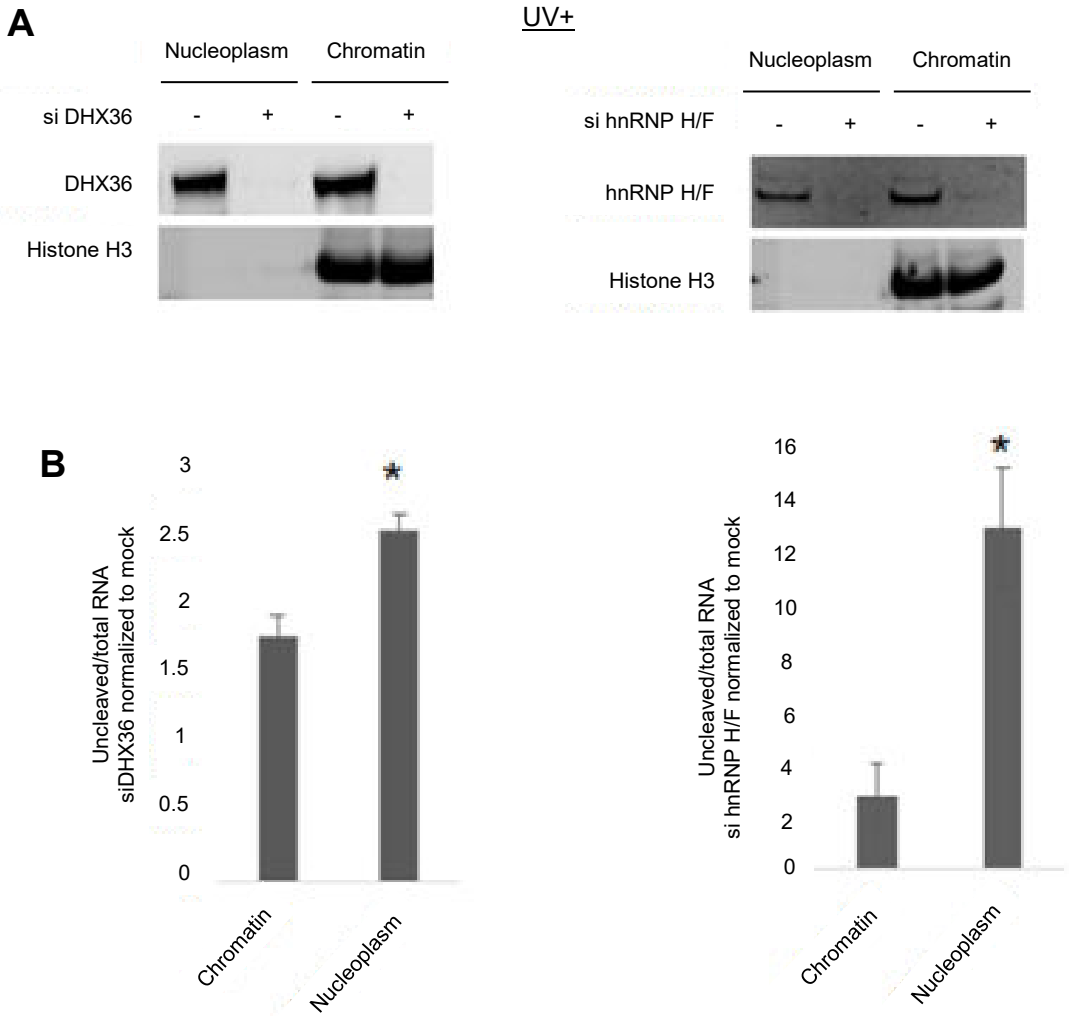

Appendix Figure S3. ***Depletion of DHX36 or hnRNP H/F inhibits p53 PAS cleavage in the nucleoplasm.*** A549 cells were transfected with siRNA against hnRNP H/F 48 hours prior to UV irradiation (40 J/m2). The nucleus was fractionated into nucleoplasm and chromatin following 16 hours of recovery. (A) The depletion efficiency was verified by western blot. (B) RT-qPCR on RNA extracted from the nucleoplasm and the chromatin fraction to quantify the uncleaved/total ratio in both fractions. (n=3 biological replicates) All data are presented as the mean ± s.e.m. *P<0.05

A

Deletion screening primer (forward)

sgRNA A

5' GTCCCTA***CCCAGCAGGCAAACTAGAG***CTCCTGAAGCTCAGTCC**CTGTCCTTGCCTCTGTAGAC**AGGTCACCTTGA 3'

3' CAGGGATGGGTCGTCCGTTTGATCTCGAGGACTTCGAGTCAGGGACAGGAACGGAGACATCTGTCCAGTGGAACT 5'

p53 CoTC element

5' TGA**GCTTCCTTTTTTTTTTTTTAATTTTTTTTTATTTTAGGCTTTATT**GGGGCATAATTGATCCCCCAAAATTGCATACA 3'

3' ACTCGAAGGAAAAAAAAAAAAATTAAAAAAAAATAAAATCCGAAATAACCCCGTATAACTAGGGGGTTTTAACGTATGT 5'

5' TTCAAGGTATGCAGTGTGATGATTTGATATGGGGGTATATTGTGAAACCATTACCACAATCAAATTAATCAGCACGTCC 3'

3' AAGTTCCATACGTCACACTACTAAACTATACCCCCATATAACACTTTGGTAATGGT**GTTAGTTTAATTAGTCGTGC**AGG 5'

sgRNA B

5' ATCATCACACACAGTTACCATTTGTGTGTGTGCACGTGTGTTCACCTACGACGAGGACACTTGGACCTACTCTGCAGAT 3'

3' TAGTAGTGTGTGTCAAGGTAAACACACACACGTGCACACAAGTGGATGCTGCTCCTGTGAACCTGGATGAGACGTCTA 5'

5' CTCAAGTAAACAGAAAATCTCCCTTTTTGACAACCATCCTCCACCCTTTCAATCCC 3'

3' GAGTTCATTTGTCTTTTAGAGGGAA***AAACTGTTGGTAGGAGGTGG***GAAAGTTAGGG 5'

Deletion screening primer (reverse)

B

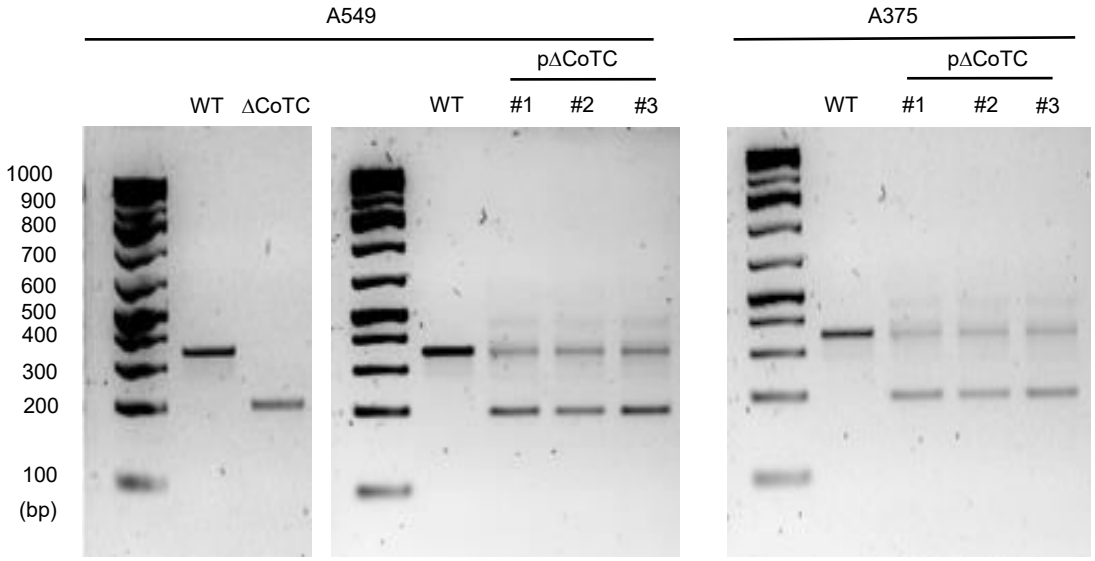

Appendix Figure S4. ***CRISPR sgRNAs were used to delete the p53 CoTC element***

A. CRISPR sgRNAs designed for the CoTC element deletion of the p53 gene.

B. PCR band profile for 'deletion' bands for gDNA from wild type (WT) and CRISPR transfected cells. The profile shows bands for complete deletion (ΔCoTC) of the p53 CoTC element in A549 cells as opposed its partial deletion (pΔCoTC) in A549 and A375 cells. (n=3 biological replicates)

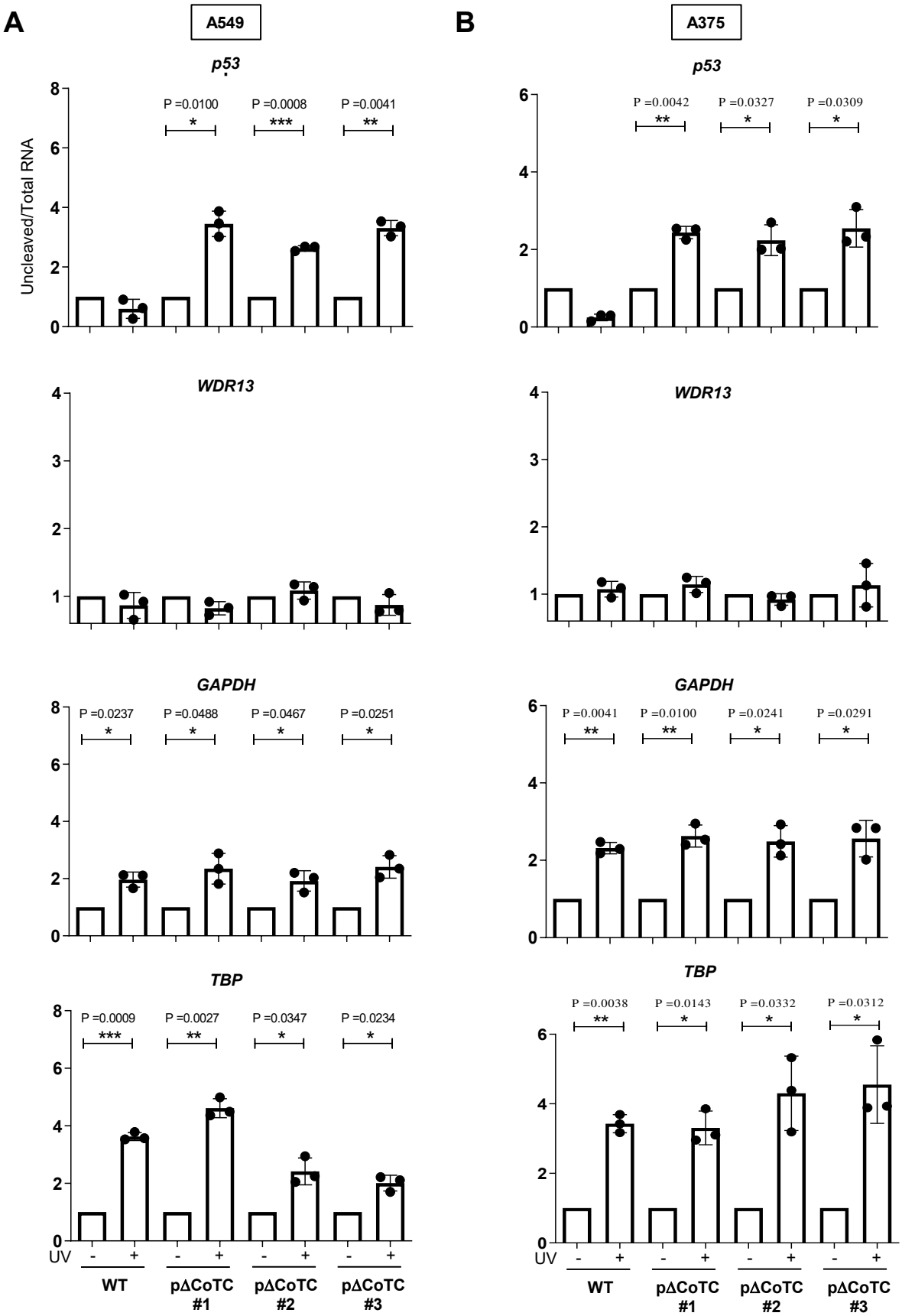
A
A549
B
A375
p53
WDR13
GAPDH
TBP
Uncleaved/Total RNA
P =0.0100
P =0.0008
P =0.0041
P =0.0042
P =0.0327
P =0.0309
P =0.0237
P =0.0488
P =0.0467
P =0.0251
P =0.0041
P =0.0100
P =0.0241
P =0.0291
P =0.0009
P =0.0027
P =0.0347
P =0.0234
P =0.0038
P =0.0143
P =0.0332
P =0.0312
UV
WT
pΔCoTC #1
pΔCoTC #2
pΔCoTC #3

Appendix Figure S5. ***Partial deletion of the CoTC element inhibits p53 PAS cleavage in response to UV .*** RT-qPCR assay on nuclear RNA for assessing the uncleaved/total ratio of p53 pre-mRNA in wild type (WT) and partial CoTC deleted (pΔCoTC) A549 (A) or A375 (B) cells (n=3) treated with or without UV irradiation (40 J/m2). "n" indicates the number of biological replicates for each experiment. All data are presented as the mean ± s.e.m. P values were calculated using two-sided unpaired t-test.

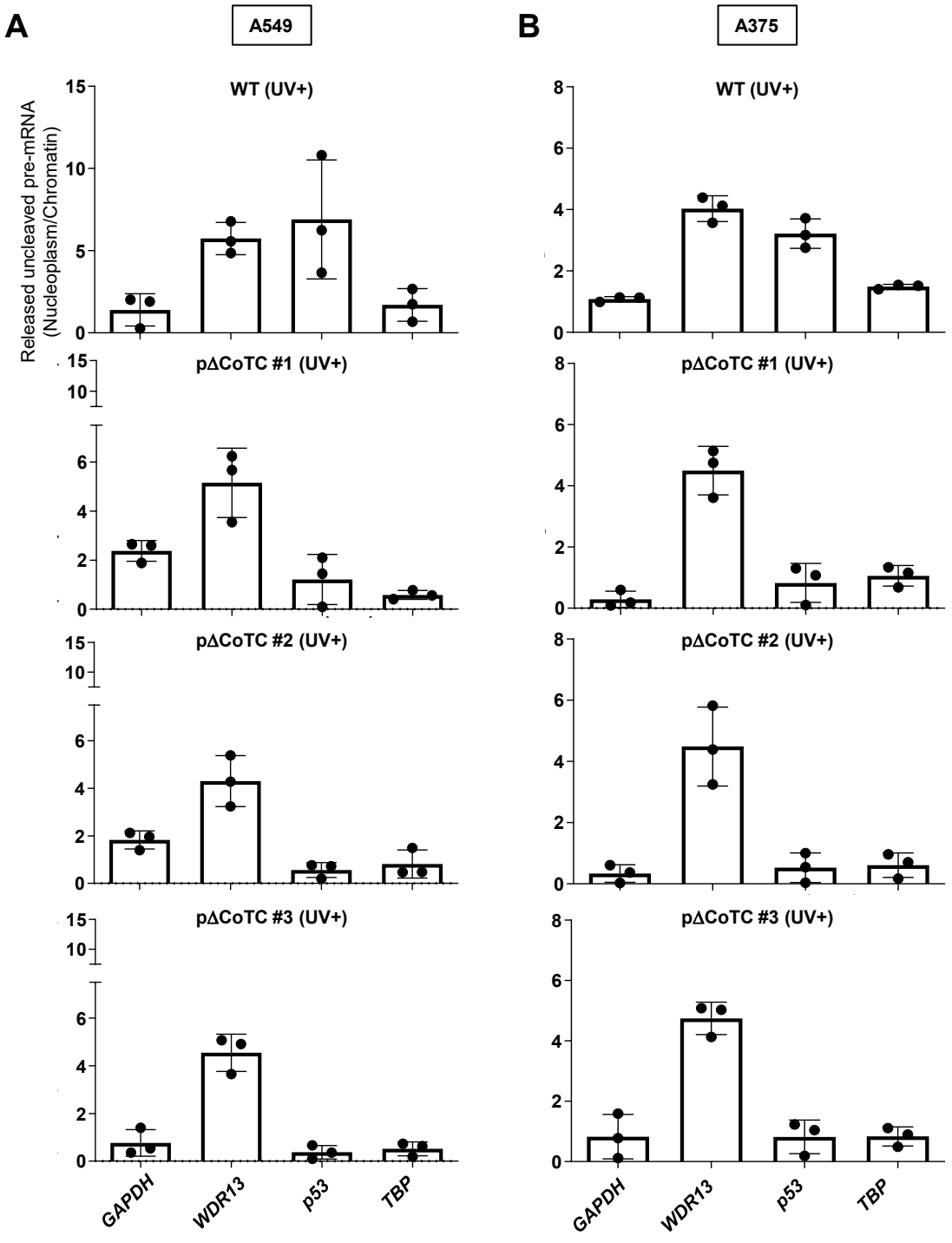
A
A549
B
A375
Released uncleaved pre-mRNA
(Nucleoplasm/Chromatin)
WT (UV+)
pΔCoTC #1 (UV+)
pΔCoTC #2 (UV+)
pΔCoTC #3 (UV+)
GAPDH
WDR13
p53
TBP

Appendix Figure S6. ***Partial deletion of the CoTC element inhibits the nucleoplasmic processing of p53 in response to UV.*** RT-qPCR analysis on RNA extracted from nucleoplasm and chromatin fractions. The ratio of uncleaved pre-mRNA (nucleoplasm/chromatin) was calculated to quantify the level of unprocessed *p53, WDR13, GAPDH* and *TBP* pre-mRNAs released in the nucleoplasm compared to the chromatin-bound unprocessed pre-mRNA in wild type (WT) and partial CoTC deleted (pΔCoTC) A549 or A375 cells (n=3) treated with or without UV irradiation (40 J/m2). "n" indicates the number of biological replicates for each experiment. All data are presented as the mean ± s.e.m.

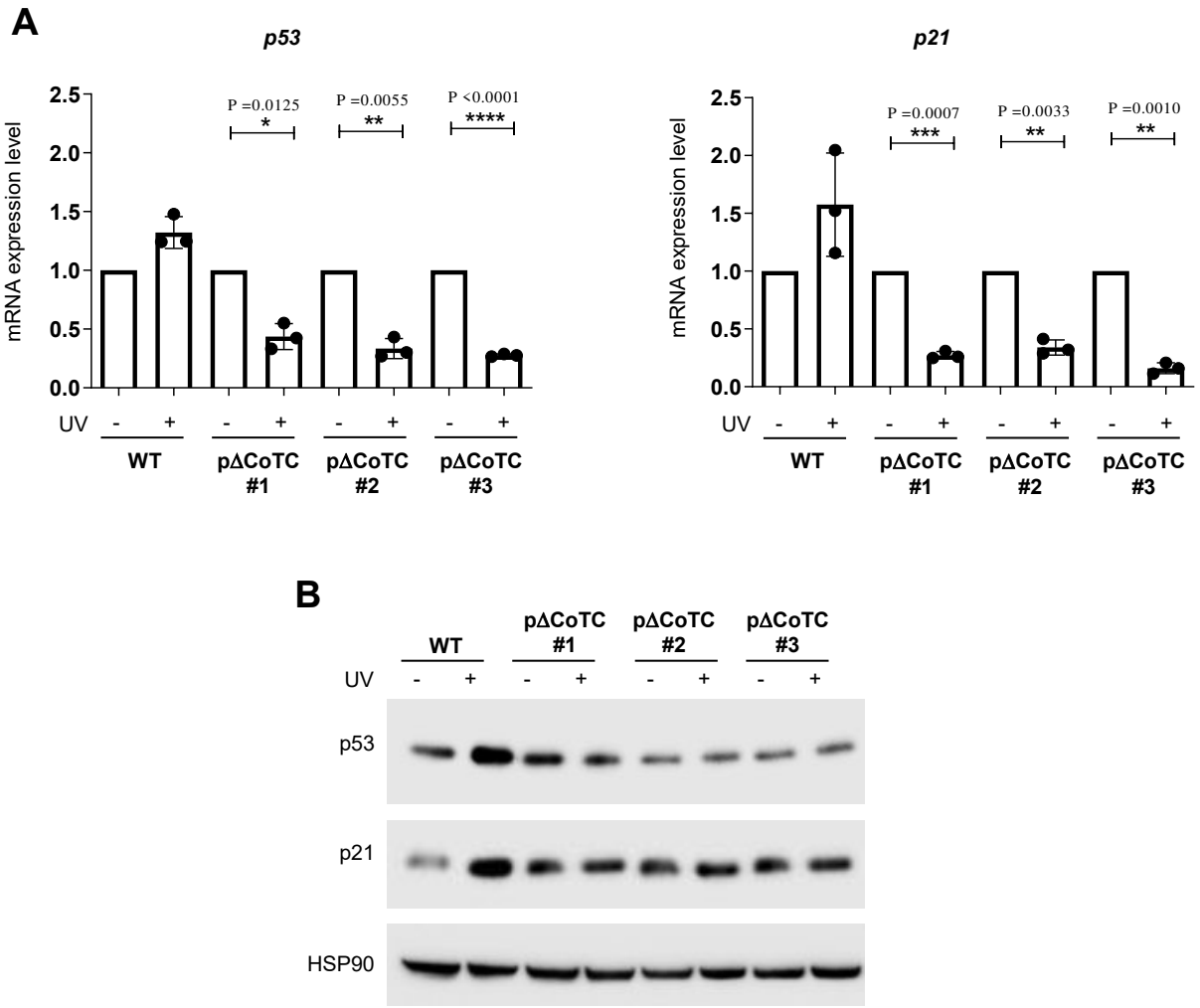

Appendix Figure S7. ***Partial deletion of the CoTC element inhibits the expression of p53 as well as p21 in response to UV***

A. RT-qPCR measuring relative p53 and p21 mRNA levels in wild type (WT) and partial CoTC-deleted (pΔCoTC) A549 cells (n=3) in response to UV treatment (40 J/m2). The expression was normalized to HPRT.

B. Western blot analysis of p53 and p21 expression wild type (WT) and partial CoTC deleted (pΔCoTC) A549 cells (n=3) treated with or without UV irradiation (40 J/m2).

"n" indicates the number of biological replicates for each experiment. All data are presented as the mean ± s.e.m. P values were calculated using two-sided unpaired t-test.

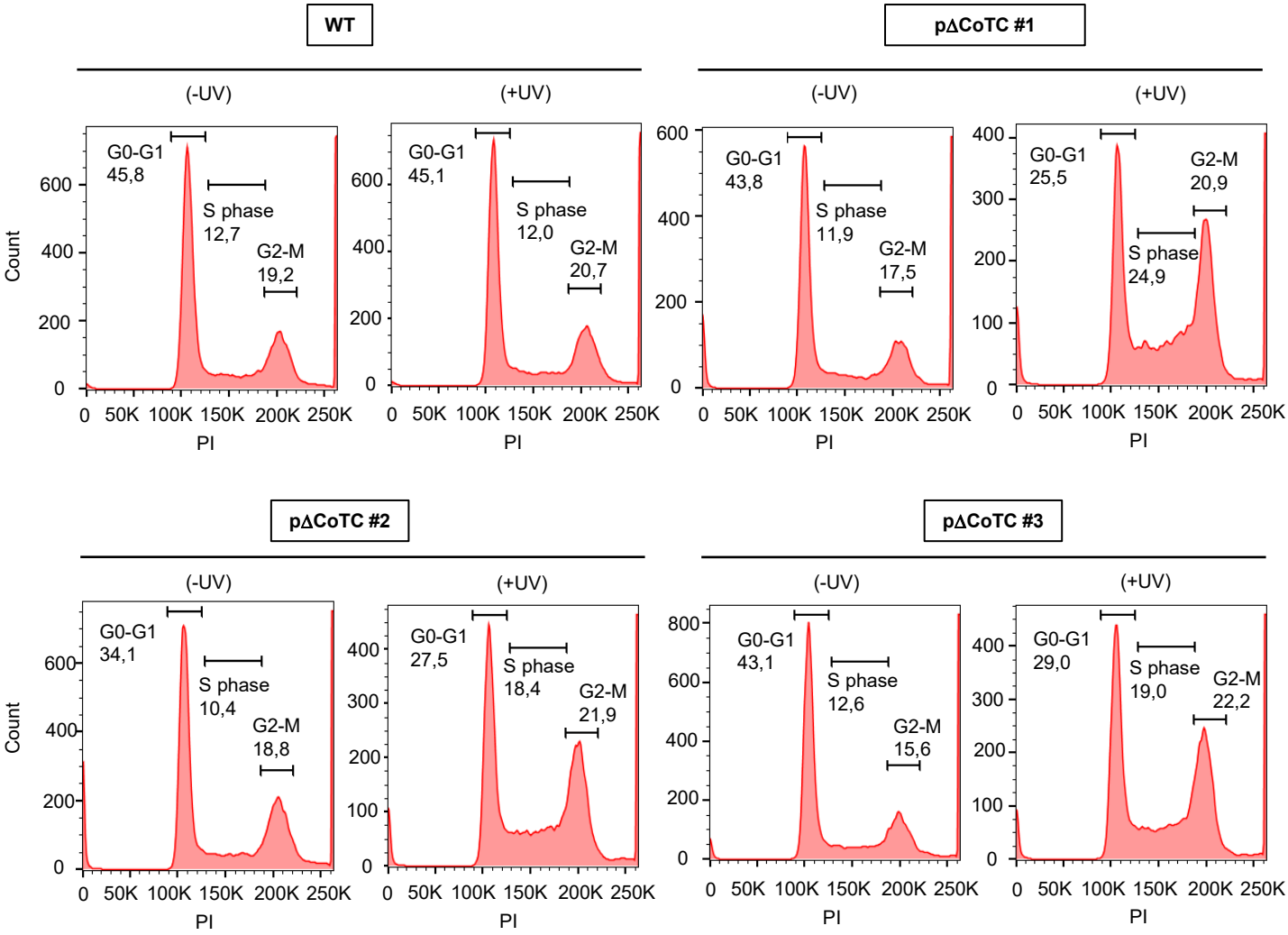

Appendix Figure S8. ***Partial deletion of the CoTC element inhibits cell cycle progression in response to UV.*** Representative flow-cytometry analyses of the cell cycle (DNA content by Propidium Iodide; PI) in wild type (WT) and partial CoTC deleted (pΔCoTC) A549 cells (n=3 biological replicates) treated with or without UV irradiation (40 J/m2).. Indicated: percent of cells in the G0-G1, S and G2/M phases.

A

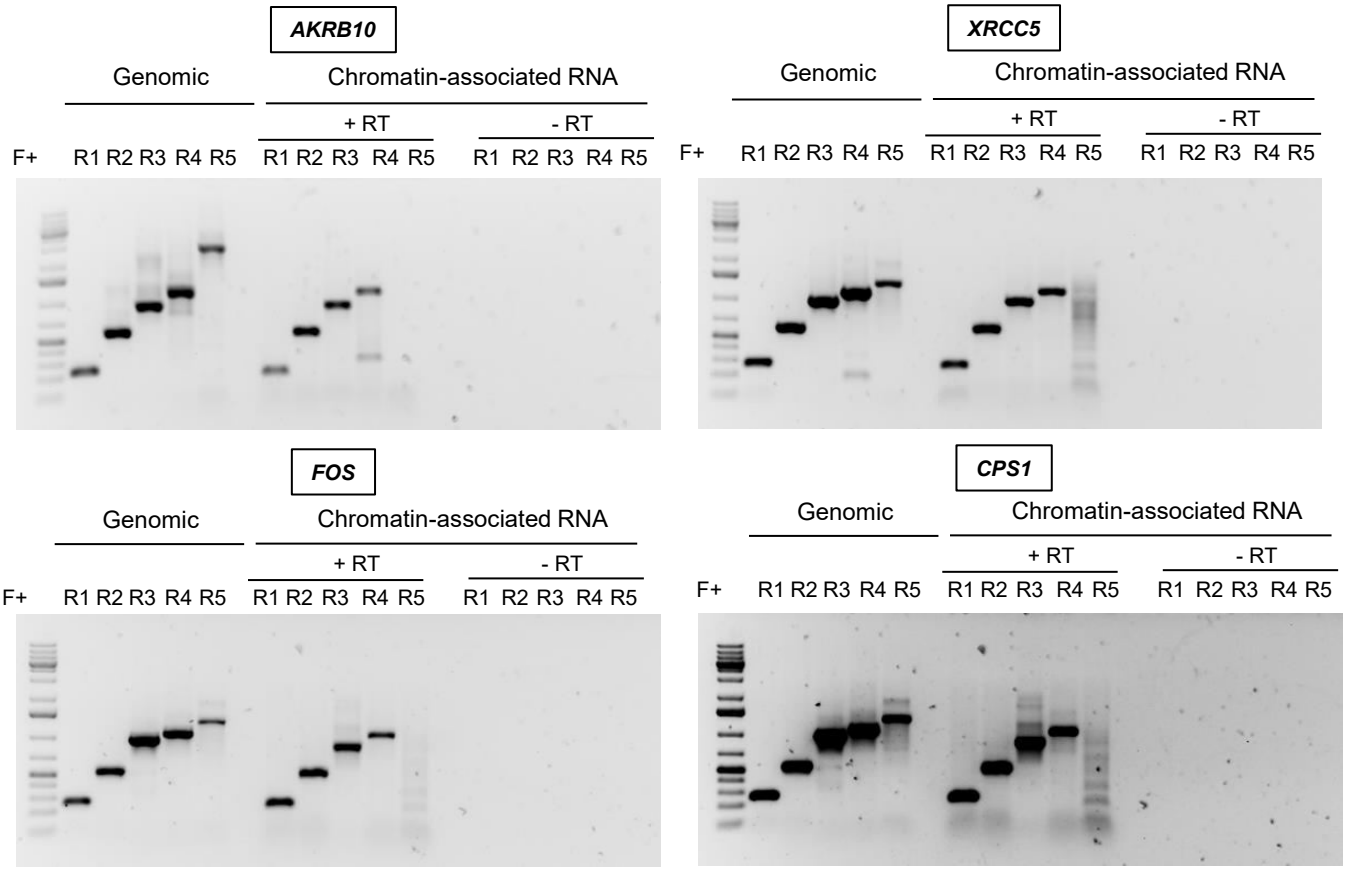
AKRB10
Genomic
Chromatin-associated RNA
+ RT
- RT
F+ R1 R2 R3 R4 R5 R1 R2 R3 R4 R5 R1 R2 R3 R4 R5
XRCC5
Genomic
Chromatin-associated RNA
+ RT
- RT
F+ R1 R2 R3 R4 R5 R1 R2 R3 R4 R5 R1 R2 R3 R4 R5
FOS
Genomic
Chromatin-associated RNA
+ RT
- RT
F+ R1 R2 R3 R4 R5 R1 R2 R3 R4 R5 R1 R2 R3 R4 R5
CPS1
Genomic
Chromatin-associated RNA
+ RT
- RT
F+ R1 R2 R3 R4 R5 R1 R2 R3 R4 R5 R1 R2 R3 R4 R5

B

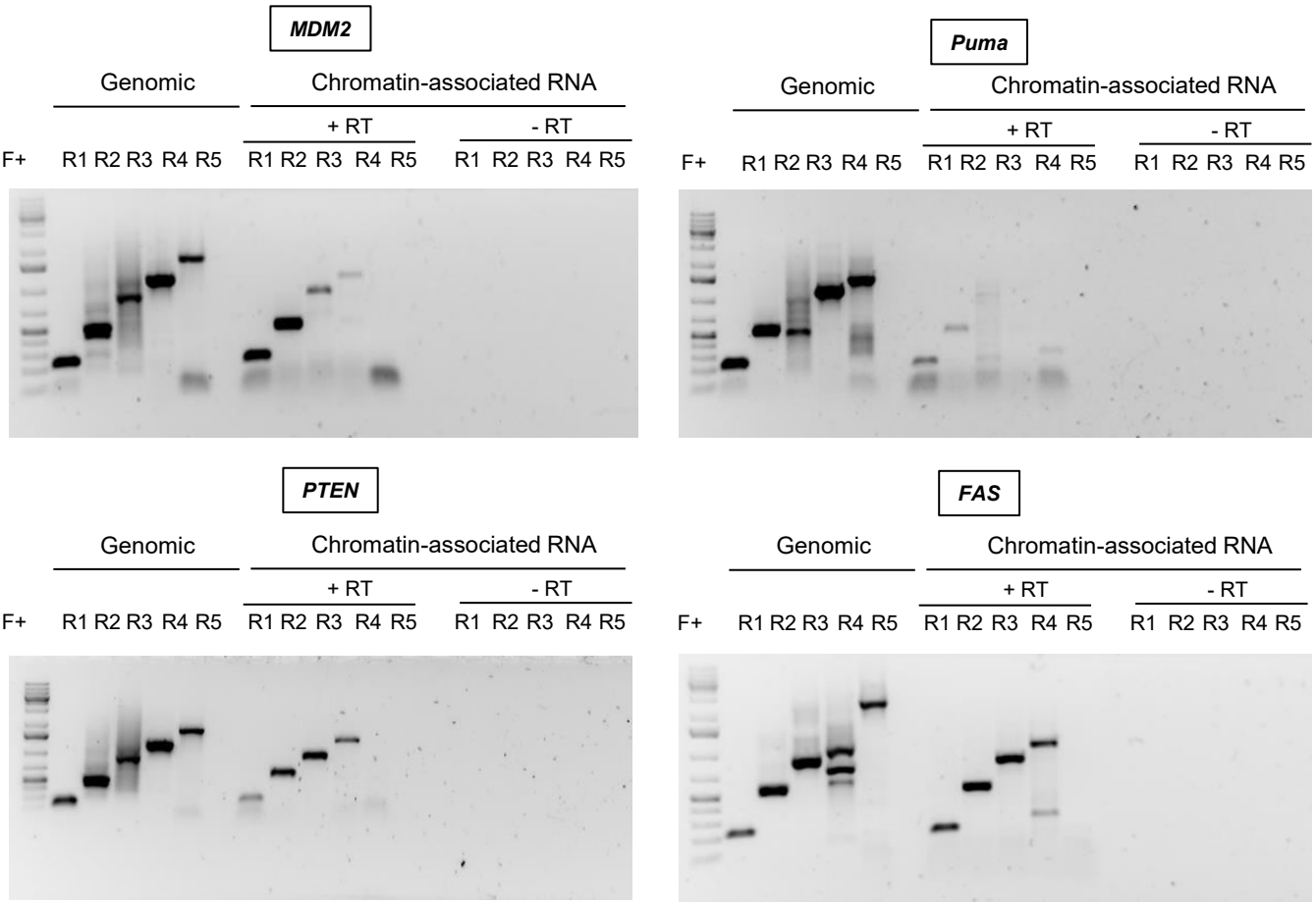
MDM2
Genomic
Chromatin-associated RNA
+ RT
- RT
F+ R1 R2 R3 R4 R5 R1 R2 R3 R4 R5 R1 R2 R3 R4 R5
Puma
Genomic
Chromatin-associated RNA
+ RT
- RT
F+ R1 R2 R3 R4 R5 R1 R2 R3 R4 R5 R1 R2 R3 R4 R5
PTEN
Genomic
Chromatin-associated RNA
+ RT
- RT
F+ R1 R2 R3 R4 R5 R1 R2 R3 R4 R5 R1 R2 R3 R4 R5
FAS
Genomic
Chromatin-associated RNA
+ RT
- RT
F+ R1 R2 R3 R4 R5 R1 R2 R3 R4 R5 R1 R2 R3 R4 R5

C

Basepairs downstream of polyA	100-200	400-600	1000-1200	1500-2000	2500-3000
MDM2	+	+	+	+	-
Puma	+	+	-	-	-
PTEN	+	+	+	+	-
FAS	+	+	+	+	-
AKRB10	+	+	+	+	-
XRCC5	+	+	+	+	-
FOS	+	+	+	+	-
CPS1	+	+	+	+	-

COTC cleavage sites between 1 – 2.5 kb downstream to the PAS.

D

Chromatin-associated RNA
(RT with oligo dT)

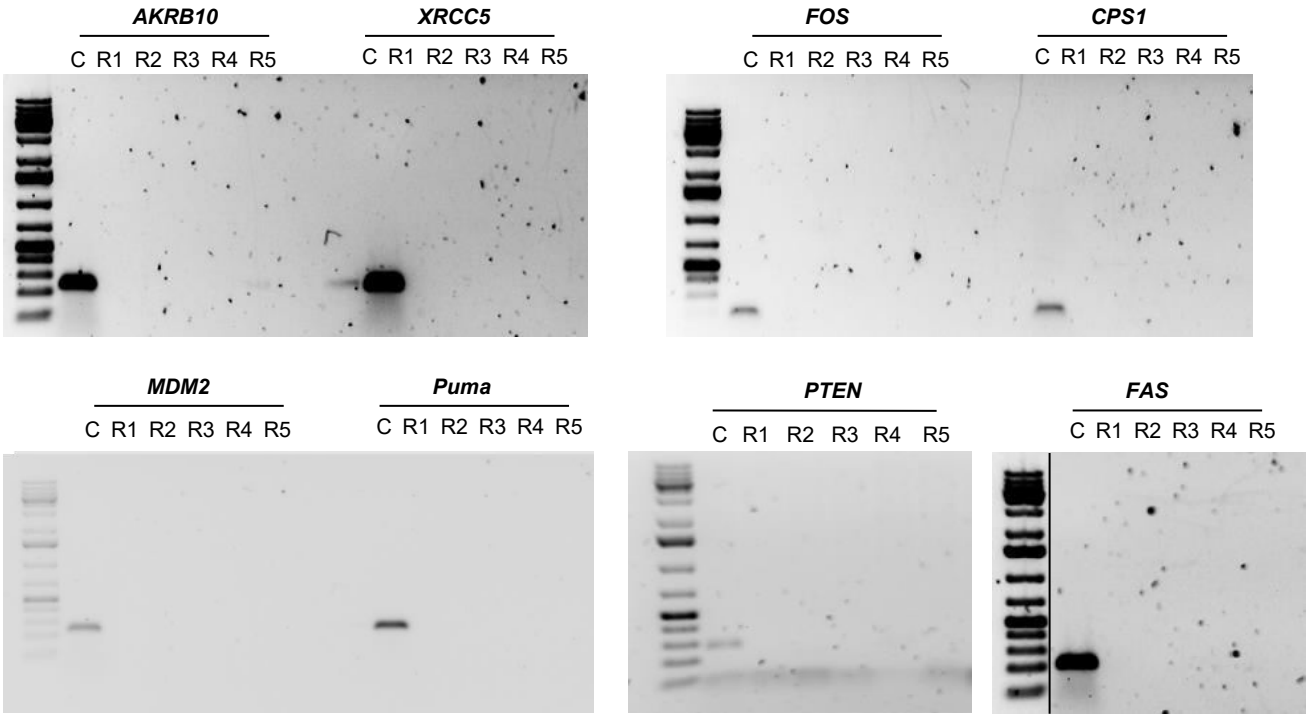

Appendix Figure S9. ***CoTC elements were identified in the 3' flanking regions of candidate genes***

A. PCR analysis of RNA seq candidate gene 3' flanking regions to map the location of CoTC elements. (n=3)

B. PCR analysis of 3' flanking regions in candidate genes from the p53 signaling pathway to map the location of CoTC elements. (n=3)

C. Table to summarize the presence or absence of bands from PCR amplification using primer pairs F/(R1-R5) in 3' flanking regions of candidate genes.

D. PCR analysis of candidate gene 3' flanking region using the same primers employed in the data panel above. Lane 1 is a control PCR amplification of cDNA derived from the reverse transcription of a control mRNA using oligo (dT). Lanes 2-6 are PCR amplification of reverse transcribed candidate gene chromatin-associated pre-mRNA using oligo oligo (dT). Likewise for all genes. (n=3)

"n" indicates the number of biological replicates for each experiment.

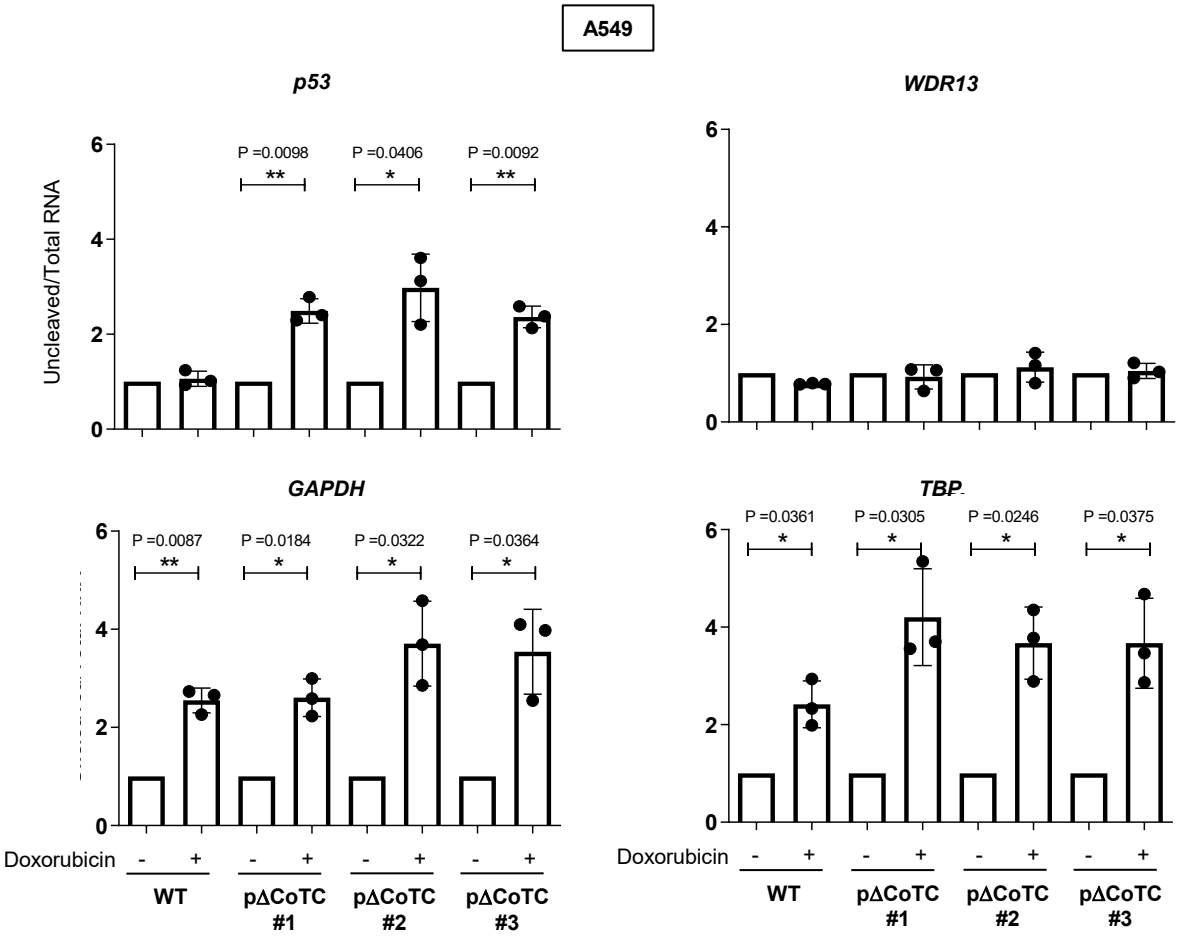

Appendix Figure S10. ***Partial deletion of the CoTC element inhibits p53 PAS cleavage in response to doxorubicin.*** RT-qPCR assay on nuclear RNA for assessing the uncleaved/total ratio of *p53* pre-mRNA in wild type (WT) and partial CoTC deleted (pΔCoTC) A549 cells (n=3) treated with or without doxorubicin (3.5 μM). "n" indicates the number of biological replicates for each experiment. All data are presented as the mean ± s.e.m. P values were calculated using two-sided unpaired t-test.

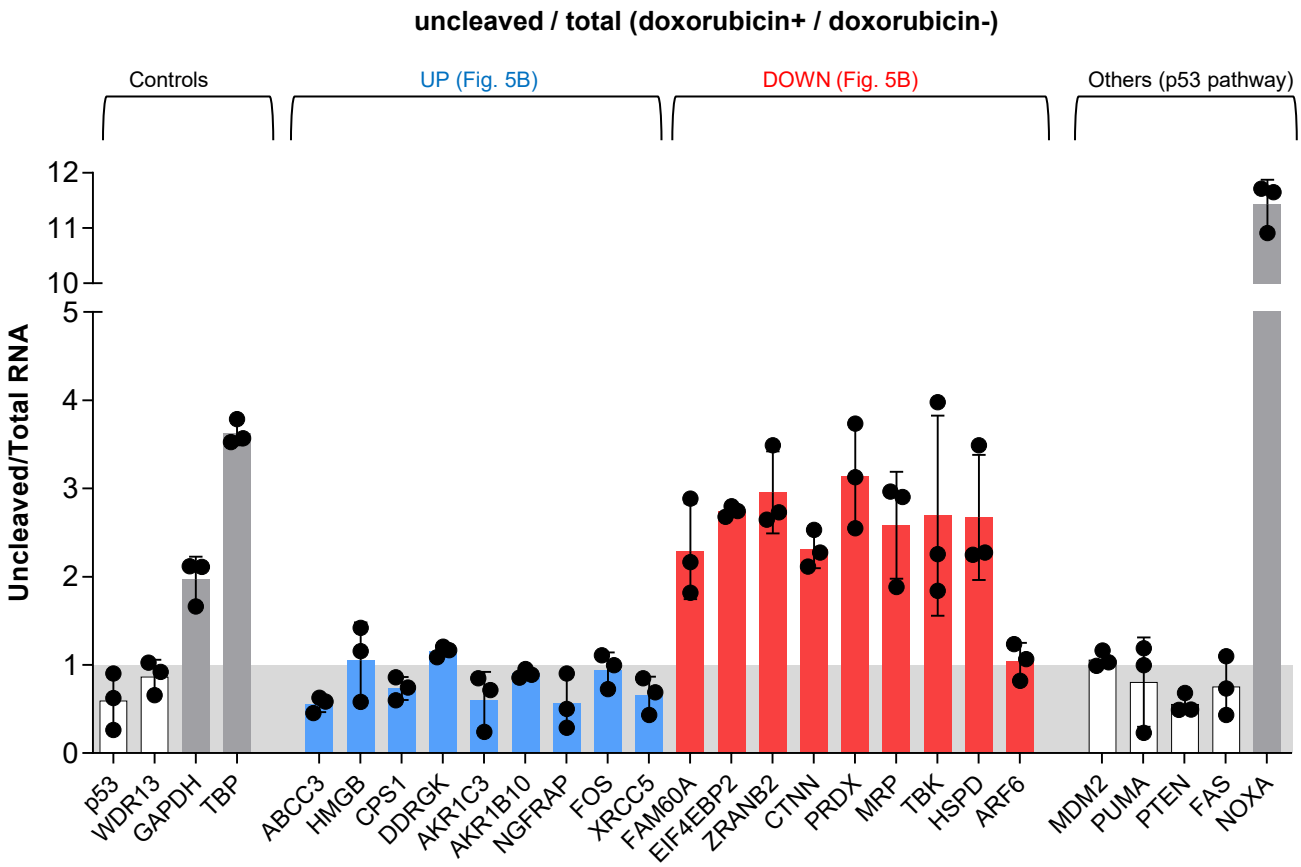

Appendix Figure S11. ***Validation of PAS cleavage inhibition of candidate pre-mRNAs in response to doxorubicin.*** RT-qPCR (uncleaved/total RNA) on nuclear RNA extracted from doxorubicin-treated or untreated A549 cells (n=3), to assess the regulation of 3'end processing of 20 pre-mRNAs randomly selected from the previous RNA-sequencing data. "n" indicates the number of biological replicates for each experiment. All data are presented as the mean ± s.e.m.

Appendix Table S1. ***siRNA sequences for all genes tested***

Gene	siRNA sequence
CPSF160	GCUUUAAGAAGGUCCCUCA
CPSF100	CUCAACUUCUUGAUCAGAU
CPSF73	CCAUAUACUGGUCCCUUUA
CPSF30	GUGCCUAUAUCUGUGAUUU
CstF77	GAAGACUUAUGAACGCCUU
CstF64	GGCUUUAGUCCCGGGCAGA
CstF50	GUCGUAAGUCCGUGCACCA
CFIm68	CUGCAAUUUCUUUAAUUAA
CFIm25	CCUCUUACCAAUUAUACUU
CFIm59	CUCAUCUGCUCGUGUGGAU
CLP1	GCUUAUGUCUCCAAGGACA
Fip1	CGAAUGGGACUUGAAGUUA
PCF11_1	GUACCUUAUGGAUUCUAUU
PCF11_2 (pool)	GAUACAAAUCAGCGACUUA
	GUGUGCAAAUUUAACGAAA
	AAGUUAAGGAAGAACGAAU
	GGAUAAGACCGAUGGCAAA
hnRNP H1	GGUAUUCGUUUCAUCUACA
hnRNP F	GGUGUCCAUUUCAUCUACA
DHX36	GGUGUUCGGAAAAUAGUAA

Appendix Table S2. ***20-mer protospacer sequences for two sgRNA and their reverse complement for the deletion of p53 CoTC***

sgRNA	**Sequence**	**Reverse complement**	**PAM**
sgRNA_A	CTGTCCTTGCCTCTGTAGAC	GTCTACAGAGGCAAGGACAG	AGG
sgRNA_B	CGTGCTGATTAATTTGATTG	CAATCAAATTAATCAGCACG	TGG

Appendix Table S3. ***Modified sgRNA sequences to facilitate cloning*****.** Protospacer sequences and their reverse complements with "CACC" and "AAAC" added for cloning into the pX458/pX459 vector using BbsI restriction enzyme

sgRNA	**Sequence**	**Reverse complement**	**PAM**
sgRNA_A	CACCGCTGTCCTTGCCTCTGTAGAC	AAACGTCTACAGAGGCAAGGACAGC	AGG
sgRNA_B	CACCGCGTGCTGATTAATTTGATTG	AAACCAATCAAATTAATCAGCACGC	TGG

Appendix Table S4. ***Primer sequences used for all genes tested***

Gene	Primer name	Sequence
Primer sequences		
TP53	Forward	AGGCGATCCACCTGTCTCA
	Reverse R1	TAGCCTGCACTGGCGTTC
	Reverse R2	TGGAGGCTCAGCCTTGCTAA
	Reverse R3	AGTACTGAGCTCCTCAACC
	Reverse R4	GAGTGTTTGGCATTCCCTAGTA
	Reverse R5	GAAGCAGCACAGCACAGCAGAAATAAA
AKRB10	Forward	TCTGCCAACACTGAGGATGT
	Reverse R1	TTGAGCAAGTTCCTCCTCCC
	Reverse R2	GGACAAACAGAAATGTTCCAGAT
	Reverse R3	ACAGGGAGAGAGGGAGAGAG
	Reverse R4	TATCACTGGGCTCTGGGTTG
	Reverse R5	GGTAAGTCTAGCCCTCTGGA
XRCC5	Forward	AGCACCCTCATAAGTCGTCA
	Reverse R1	TGAGCACCTGTATGTCAAGTT
	Reverse R2	GCACAAATAATCCTGCTGCA
	Reverse R3	ACTGGCAAAGGATTAAAACCCA
	Reverse R4	TGTACTCCAGCCTCGGTG
	Reverse R5	CTCTGCCTCCCAAAGTGCT
FOS	Forward	TGTTTGCTTATTGTTCCAAGACA
	Reverse R1	CGTCCCCAGAAGCAGTAGAA
	Reverse R2	GCAGGAAGATTCTAATGCCGA
	Reverse R3	ACGATCAGCCATTATTTGTGC
	Reverse R4	TGAACAGCAAACAGGGATCC
	Reverse R5	TTGAGGTCAGGAGTTCGAGG
CPS1	Forward	AGGGCAGCCTTTGTTACTTT
	Reverse R1	AGCAAGGGAGGGACAAGAAA
	Reverse R2	TGGTAATCAATTGACTGTGAGGT
	Reverse R3	ATGGTGATGGTGGTTGTGGT
	Reverse R4	CAGCCTGCTCACTTTTAGTCA
	Reverse R5	CATTGTTCAAGAGGCTGTGGA
MDM2	Forward	AGGTAGATATCTGAAAGCACCA
	Reverse R1	TGTTTCAGTACCACTCCTCTCT
	Reverse R2	GGAGGTTGAGGCTGTAGTGA
	Reverse R3	CTCACGCCTGTAATCCCAGT
	Reverse R4	TGGGGAGGTGTGAACCAAAA
	Reverse R5	CTTCAAGGTGGAGTAGGGGT
Puma	Forward	CGCTGCTGTAGATACCGGAA
	Reverse R1	GCCTTTCTTCTGATGGAGCC
	Reverse R2	GGCTTGATCATCGCTCACTG
	Reverse R3	CGTCTCGATCTCCTGACCTC
	Reverse R4	GCTCGCTGTAACCTTTATCTCC
	Reverse R5	CGTACAGTGGTGCAATCTCG
PTEN	Forward	AATGCCTCATCCCAATCAGAT
	Reverse R1	TTCTGAACTAGCAACAGCACT
	Reverse R2	TGTTGTTGTGATGGGGAAGT
	Reverse R3	AGCCACTGAATTCGAAAGGA
	Reverse R4	ACGCGGTAATTTTCAGAGCT
	Reverse R5	GCCTCACTTCATTCCACACA
FAS	Forward	TTTGCCCCTTGTGTTTGGAA
	Reverse R1	TGTGCTGTTTGGAAGAGGTC
	Reverse R2	GGAACCCTAAGCAAAGCACA
	Reverse R3	CCACCACAAAGAGAACCAGG
	Reverse R4	AGCAGACATAATCAACAGCAACA
	Reverse R5	TCCTAAAATGCAACATACGGAGA
PCF11	Forward total	AGCCGAAAAGTCACTCATAGAC
	Reverse total	GCCTCTTGAGTTTTGAGCAC
TP53	Forward total	AGGCGATCCACCTGTCTCA
	Reverse total	CAGATGTGCTTGCAGAATGT
	Forward uncleaved	AGGCGATCCACCTGTCTCA
	Reverse uncleaved	TAGCCTGCACTGGCGTTC
TBP	Forward total	GGAAGGGGCATTATTTGTG
	Reverse total	GCCCAGATAGCAGCACGGTA
	Forward uncleaved	GCAGGACAGAATATATGTGTTAATG
	Reverse uncleaved	CAGTATGATCACATGACTCTTACAAGG
	Forward total	CATGGTCATCGTCTGGAGGC
	Reverse total	TAAGAGGGGTGGGATGGAGG

WDR13	Forward uncleaved	CATTCATGCATCGACGGATTC
	Reverse uncleaved	TAGAACAGTTCCTGGCACAC
GAPDH	Forward total	CCAAGGAGTAAGACCCCTGG
	Reverse total	GTACATGACAAGGTGCGGC
	Forward uncleaved	TACCCTGTGCTCAACCAGTTA
	Reverse uncleaved	CAGCTTCCTGTAGCACTCAA
ABCC3	Forward total	AACAGAAGACAGCTGCTGGG
	Reverse total	AATGGATTCAGGCAGCACCC
	Forward uncleaved	CAGTAGTCTTTTTGCACTTGTTCAC
	Reverse uncleaved	GTAGAAAGTCTTCCTCTTGGCCT
HMGB1	Forward total	TCGTCCCATCACAGTGTTGTT
	Reverse total	CTCGGGTACACAGGACACAC
	Forward uncleaved	GCGCCCATGTAACACAAACT
	Reverse uncleaved	TCCTACAATGTCTGAGCAATGG
CPS1	Forward total	TTCCCTTAAGACGATGGATTCTG
	Reverse total	TGTAGAAGGAATGGTGTCCTTG
	Forward uncleaved	AGGGCAGCCTTTGTTACTT
	Reverse uncleaved	AAACCAGATTCAACTGCATTACC
DDRGK1	Forward total	TGGTGTGGCTTGGTGTG
	Reverse total	AACAGGACTTCACCAGCTTC
	Forward uncleaved	AAATAGCCTGTTGCACATTTACTC
	Reverse uncleaved	TTAACAGAGATGTGGCCCAAG
AKR1C3	Forward total	CTGAGTCCATAGGCCAGAAAG
	Reverse total	ACACTACAGAACAGAGTAGGTAAAG
	Forward uncleaved	CCTACTCTGTTCTGTAGTGTGTG
	Reverse uncleaved	CCCTGTTGAGCCAGAAGAAA
AKR1B10	Forward total	GACGAGAATCGAGGTGCTGT
	Reverse total	TCAAGCCATGCTTTTCTGTGAT
	Forward uncleaved	GCGATCGATGGTCATCCTCTT
	Reverse uncleaved	GAAGGCAAGCTGTGAGAGCA
NGFRAP	Forward total	CCATGTGTCAAGTGGGTCTT
	Reverse total	CCATGCAAATGGGTGAAACTAC
	Forward uncleaved	CACTAGAGTGTTAATTGGTGAACAT
	Reverse uncleaved	ATCTCCTGACCTCGTGATCT
FOS	Forward total	TTGTTGAGGTGGTCTGAATGT
	Reverse total	CTTGGAACAATAAGCAAACAATGC
	Forward uncleaved	AGTTGAATGCGACCAACCT
	Reverse uncleaved	GTCCTCTTTGATAAGGGATCAGAC
XRCC5	Forward total	TTGTGGATGGTGTCTCCTTTAC
	Reverse total	CACCAAAGAGGAACTGGAACT
	Forward uncleaved	GCTGAGAATTGAACACCCTTATC
	Reverse uncleaved	GATGTCCTAGAAGCCCAAAGTA
FAM60A	Forward total	GCTGCAGTATTGGTGGTAGAA
	Reverse total	CAGTACATCCTACAGGCAAAGAG
	Forward uncleaved	GTACTGTATGTAGTCATGCACTTTG
	Reverse uncleaved	CCTGTCAAACAAAGCCACAA
EIF4EBP2	Forward total	TGTCTCCCATGATGTGTTGTT
	Reverse total	CACACAGGACTGCCTCAAG
	Forward uncleaved	TTCTGGTGAAATCCTGCTAAGG
	Reverse uncleaved	AGTGTGGAGAACTGACAGATAAAG
ZRANB2	Forward total	GCTGTACTAAGCAAATGCAAGG
	Reverse total	TGCTTGACTCACAGGCTTTAT
	Forward uncleaved	ATTCCAAAGCCATTATCACTGC
	Reverse uncleaved	TCAGGAAGCACACTACGATATG
CTNNB1	Forward total	GTATGGGTAGGGTAAATCAGTAAGAG
	Reverse total	TCTCTTGAAGCATCGTATCACAG
	Forward uncleaved	CTGTGATACGATGCTTCAA
	Reverse uncleaved	ACCACCCTCACAAACCATTTA
PRDX6	Forward total	TTCCGATGATGTGTACATGAAAGA
	Reverse total	AAATAGCAACCCACTGCAAGA
	Forward uncleaved	GGGTCAGAGAATTCTGTTGTCATA
	Reverse uncleaved	CACGTTCTTCAGCTGTTCCT
MRPL32	Forward total	GGAAGATTCTTTATGTTGTTGTGCT
	Reverse total	AATCCATTGAGCCTTTGGATAAAC
	Forward uncleaved	CCAAAGGCTCAATGGATTATGT
	Reverse uncleaved	AAAGGCACTGGCAAACAAA
TBK1	Forward total	CAGAACCGCACCACTGTTA
	Reverse total	GGATACAAGGATAACTGGGATCTG
	Forward uncleaved	AGAGTTCATGTGTTTCTTTGTATCC
	Reverse uncleaved	TTGTCCCTAGATCCAATATTCTGAG
	Forward total	ACCAGTGTACTGCTTTCAACT
	Reverse total	AAGGCTGCTTAACTTCTCATCT

HSPD1	Forward uncleaved	GATGAGAAGTTAAGCAGCCTTTC
	Reverse uncleaved	CTCCCAAGTAGCTGGGATTA
ARF6	Forward total	GAAACACAGCAGTTCTTGGTAAAG
	Reverse total	AGCCATCTACAGCAAGTGATAAG
	Forward uncleaved	ACTATGTTGCAAGTCTGTTTCATC
	Reverse uncleaved	CCACTGTGGGCTAAGTTTACTA
MDM2	Forward total	CGCTTTATGGGTGGATGCTG
	Reverse total	ATTGAAAGCTGGCTACATGGT
	Forward uncleaved	CACCAGCACTTGGAAGGTGT
	Reverse uncleaved	GAGTACAGCAATCATTTCAGATGC
PUMA	Forward total	GAGATTTTGGCTGAAGCCGC
	Reverse total	CAGTATCTTACAGGCTGGGC
	Forward uncleaved	GCTGCTGTAGATACCGGAATGA
	Reverse uncleaved	AGGGAAGGCAAGCAGAAAGA
PTEN	Forward total	AGCAGTGGCTCTGTGTGTAA
	Reverse total	CATCTGATTGGGATGAGGCA
	Forward uncleaved	TCTTGTCATTGTGTGGGTGT
	Reverse uncleaved	AGGCTTTGAAGGACAGCAGG
FAS	Forward total	AGCAGATACCTGGAACCACC
	Reverse total	TTATAATTCCAAACACAAGGGGC
	Forward uncleaved	AGCAGATACCTGGAACCACC
	Reverse uncleaved	GAGTACAGCAATCATTTCAGATGC
NOXA	Forward total	AGGTTGTAGTCACTTTAGATGGAA
	Reverse total	TACCAGATGGTAAAATAGCTGCCT
	Forward uncleaved	AAGTTGATACTGTGGCAGTAAAC
	Reverse uncleaved	GTCTGCTGATGGAAATCAGTTAAA